Changes in wave climate over the northwest European shelf seas during the last 12,000 years

S. P. Neill,[1] J. D. Scourse,[1] G. R. Bigg,[2] and K. Uehara[3]

S. P. Neill, School of Ocean Sciences, Bangor University, Marine Science Laboratories, Menai Bridge, LL59 5AB, UK. (s.p.neill@bangor.ac.uk)

J. D. Scourse, School of Ocean Sciences, Bangor University, Marine Science Laboratories, Menai Bridge, LL59 5AB, UK. (j.scourse@bangor.ac.uk)

G. R. Bigg, Department of Geography, The University of Sheffield, Sheffield, S10 2TN, UK. (grant.bigg@sheffield.ac.uk)

K. Uehara, Research Institute for Applied Mechanics, Kyushu University, Kasuga, Fukuoka 816-8580, Japan. (uehara@riam.kyushu-u.ac.jp)

[1]School of Ocean Sciences, Bangor

Abstract. Due to depth-attenuation of wave orbital velocity, wave-induced bed shear stress is much more sensitive to changes in total water depth than tidal-induced bed shear stress. The ratio between wave- and tidal-induced bed shear stress in many shelf sea regions has varied considerably over the recent geological past due to combined eustatic changes in sea level and isostatic adjustment. In order to capture the high frequency nature of wind events, a two-dimensional spectral wave model is here applied at high temporal resolution to time slices from 12 ka BP to present using paleobathymetries of the NW European shelf seas. By contrasting paleo wave climates and bed shear stress distributions with present-day conditions the model results demonstrate that, in regions of the shelf seas which remained wet continuously over the last 12,000 years, annual root-mean-square (rms) and peak wave heights increased from 12 ka BP to present. This increase in wave height was accom-

University, Marine Science Laboratories,
Menai Bridge, LL59 5AB, UK.

[2]Department of Geography, The
University of Sheffield, Sheffield, S10 2TN,
UK.

[3]Research Institute for Applied
Mechanics, Kyushu University, Kasuga,
Fukuoka 816-8580, Japan.

panied by a large reduction in the annual rms wave-induced bed shear stress, primarily due to a reduction in the magnitude of wave orbital velocity penetrating to the bed for increasing relative sea level. In regions of the shelf seas which remained wet over the last 12,000 years, the annual mean ratio of wave- to (M_2) tidal-induced bed shear stress decreased from 1 (at 12 ka BP) to its present day value of 0.5. Therefore, compared to present-day conditions, waves had a more important contribution to large-scale sediment transport processes in the Celtic Sea and the northwestern North Sea at 12 ka BP.

1. Introduction

The repeated flooding and emersion of the continental shelves driven by Quaternary glacio-eustatic cycles of up to $115 - 135$ m [*Milne et al.*, 2002] has been described as *... the most important geologic event of recent time ...* [*Newell*, 1961]. The areal extent of the shelf seas (< 200 m deep) is now 425% greater than during the Last Glacial Maximum (LGM), 7% of the total global sea-surface. The changes in relative sea level over the last deglacial transition were largely driven by glacio-eustatic, glacio-isostatic and ice-water gravitational attraction mechanisms [*Mitrovica et al.*, 2001], and had a profound impact on the hydrodynamic evolution of the shelf seas. The tidal dynamic feedbacks, with implications for tidal amplitudes, bed shear stress and sediment dynamics, are under active investigation via geologically-constrained paleotidal models [*Austin*, 1991; *Hinton*, 1995, 1996; *van der Molen and de Swart*, 2001b; *Uehara et al.*, 2006; *Rippeth et al.*, 2008; *Scourse et al.*, 2009]. Although tidal currents dominate long-term sediment movements over shelf seas [*Pingree and Griffiths*, 1979], waves also have an important contribution [e.g. *Ogston and Sternberg*, 1999; *van der Molen*, 2002]. Due to attenuation of wave motion with depth, the magnitude of wave-induced bed shear stress (τ_w) is much more sensitive to variations in total water depth, in contrast to tidal-induced bed shear stress (τ_0). For example, a typical wave height of 3 m with wave period 8 s will result in a relatively high bed shear stress of 2.02 N m^{-2} in 20 m water depth, reducing to 0.37 N m^{-2} in 50 m water depth and 0.04 N m^{-2} in 100 m water depth. Therefore, wave-induced bed shear stresses have varied considerably from the Late-glacial to present, due to a corresponding change in sea level and isostatic/eustatic adjustment over this time period [*Peltier*, 2002].

In addition, the astronomical tide-generating forces have been relatively constant over the last 12,000 years [*Berger et al.*, 1992]. In contrast, wind climate, and hence the resulting wave climate, has varied considerably over this period [*Renssen et al.*, 2007]. Indeed, even within the decadal timescale of present-day wind conditions, there is considerable inter-annual variability in wind (and resulting wave) climates [*Hurrell and van Loon*, 1997]. Consideration of wave-induced bed shear stress, in addition to tidal-induced bed shear stress, provides a more accurate representation of net bed shear stress and hence sediment transport processes in shelf seas. Further, wind waves are the dominant cause of sediment entrainment in many regions of shelf seas with low tidal energy [e.g. *van der Molen*, 2002] and, since wind forcing is independent of tides, generally accelerate the magnitude of sediment transport and hence the rate of bed level change [*Vincent et al.*, 1998]. An estimate of how the ratio between wave- and tidal-induced bed shear stress at shelf scale has varied since the Late-glacial provides a useful tool with which to analyze bedforms and constrain the timing of sediment deposition events/regimes observed in sediment cores recovered from shelf seas.

A simple point model, based on a binned time series wind climate applied to a JONSWAP spectrum, has been applied to paleo time slices of the southern North Sea, demonstrating that mean wave heights in this region increased from 7.5 ka BP to present [*van der Molen and de Swart*, 2001a]. Application of sediment transport formulae to wave model output suggested that in this region (where present-day water depths are of order $30-50$ m), the mode of wave-induced sediment transport changed from dominantly suspended transport prior to 6 ka BP to dominantly bed-load transport thereafter, due to sea-level rise. These simulations were made on the assumption that wind climate was invariant over

the Holocene, and neglected refraction and non-linear wave-wave interactions. As far as the authors are aware, this is the only published work on paleowave modeling, particularly with application to sediment transport processes over any region at shelf scale. Further, neither inter-annual variability or annual estimates of mean and peak wave conditions at shelf scale have been estimated for paleo time slices.

In this paper, a two-dimensional (2D) spectral wave model is applied to the NW European shelf seas for a decade of wind-forcing at synoptic-scale variability. Initially, the model is validated using present-day bathymetry, providing a benchmark for comparison with subsequent paleo-simulations. The model is then applied to a series of paleobathymetries from 12 ka BP to present. The degree of sensitivity of model results to bathymetry or atmospheric forcing is tested by examining the response of the model at each time slice to a wide inter-annual variability in the decade of predicted wave climates, ranging from conditions representative in character of much colder climates to warmer climates than present. Finally, bed shear stress output by the wave model for time slices from 12 ka BP to present is contrasted with tidal-induced bed shear stress output from a paleotidal model study of the same region [*Uehara et al.*, 2006]. The application of this work is to assist in analysis of bedforms and constraining the timing of sediment deposition events/regimes over the NW European shelf seas through the Late-glacial and Holocene.

2. Study Area

The NW European shelf seas are located on the northeastern margin of the North Atlantic and are generally shallower than 200 m (Figure 1). The Celtic Sea, Malin Sea and northern North Sea are exposed to Atlantic waters, with water depths in the range $100-200$ m, with the exception of the deeper (600 m) Norwegian trench in the northeastern

North Sea. The Celtic Sea borders the Irish Sea to the north, a semi-enclosed water body containing a north-south orientated channel of depth 250 m. To the east of the Celtic Sea, the English Channel connects to the southern North Sea. This region of the North Sea is generally shallower than 50 m, and contains various large sandbanks, the most prominent of which is Dogger Bank. Substantial crustal rebound occurred over the NW European continental shelf due to unloading of the local British and Fennoscandian ice sheets [*Peltier*, 1994; *Lambeck*, 1995]. These ice sheets had ablated by 9 ka BP and their deglaciation was a major source of sediment supply to the NW European shelf seas [*Boulton et al.*, 1985; *Cameron et al.*, 1987; *Scourse et al.*, 2009], with a significant role in the formation of large sand banks such as Dogger Bank [*Carr et al.*, 2006].

The climate of the NW European shelf is dominated by the polar front [*Palutikof et al.*, 1997]. The instability of this front causes depressions to form, tracking across the North Atlantic and following a preferred route which passes between Iceland and Scotland. As these depressions move across the Atlantic, they follow a life cycle which, by the time they reach the British Isles, means that they are generally in a phase of maturity or decay. There is considerable variation in the wind climate around the NW European shelf seas, but the strongest winds generally emanate from the west and south, and the mean winds from the southwest [*Barrow and Hulme*, 1997]. Wind speeds tend to be highest to the northwest of the British Isles (closest to the depression tracks), decreasing towards the south and east. An annual cycle of higher wind speeds in winter and lower speeds in summer reflects the seasonally varying strength of the large-scale atmospheric circulation [*Palutikof et al.*, 1997]. Inter-annual variability in the synoptic-scale circulation over the Atlantic is described by the North Atlantic Oscillation (NAO) index, which

exhibits considerable inter-annual variability. The strong background flow leads to high mean wave energy over the shelf seas and the variability results in a wave climate with considerable extremes [*Draper*, 1980]. In regions of the shelf seas exposed to the Atlantic, the orbital velocity, and hence wave-induced bed shear stress, of the longer-period (swell) waves penetrates to the sea bed. Where fetch length is sufficient, the wave distribution over the shelf seas broadly follows the wind distribution [*Draper*, 1980]. Due to the dominant southwesterly wind direction, many regions of the NW European shelf seas are relatively sheltered from wind effects and hence experience relatively low wave energy, particularly the western seaboard of the North Sea (sheltered by the UK land mass) and the northern half of the Irish Sea (sheltered by Ireland).

3. Data

3.1. Bathymetry Data

The relative sea-level data were supplied by Kurt Lambeck every 1 ka from 12 ka BP to present, based on a glacio-isostatic adjustment (GIA) model of *Lambeck* [1995], updated to incorporate recent advances in ice-sheet modeling and crustal-rebound formulation [c.f. *Lambeck and Chappell*, 2001; *Lambeck and Purcell*, 2001; *Lambeck et al.*, 2003]. Since glacio-isostatic (un)loading history can result in profound vertical crustal movement, in particular over formerly glaciated continental shelves, this approach is more realistic than assuming solely eustatic sea-level changes as in early tidal modeling experiments [e.g. *Austin*, 1991].

Paleobathymetry data at each time slice were derived by combining the relative sea-level information with a present-day bathymetry, defined on the same horizontal grid. Grid resolution of the bathymetry time slices is $1/12^\circ$ in both latitude and longitude

(∼ 7 km) and the domain extends from 15°W to 15°E and from 45°N to 65°N (Figure 1). Bathymetries for selected paleo time slices are plotted in Figure 2. The derivation of the paleo and present-day bathymetry data are described in more detail in *Uehara et al.* [2006].

3.2. Wind Data

The source of synoptic surface wind fields was the ECMWF-ERA-Interim reanalysis [*Simmons et al.*, 2006], available at a (global) grid resolution of 1.5°, with a time step of 3-hours from 1989-1998, a decade which witnessed considerable variability in the NAO (Table 1), and hence considerable inter-annual variability with which to examine extremes in the wave model. The ECMWF-ERA-Interim analysis differs from previous reanalysis products (i.e. ERA-15 and ERA-40) in that it includes 4D-Var (or data assimilation in time as well as all three spatial dimensions) and has improved horizontal resolution (T255 ∼ 80 km in contrast to T159 ∼ 125 km for ERA-40). The data available to the user is at a similar resolution to the previous ERA-40 and ERA-15 datasets, but the original analysis is at a better resolution, hence the standard gridpoint data should represent the observed atmosphere better. For present-day validation of the wave model, one year of wind data was obtained from six meteorological stations, each in relative proximity to six corresponding waveriders (Table 2). In situ wind data were used for the validation exercise in order to resolve more accurately the high frequency (generally half-hourly) wave observations (section 3.3). The wind data is hourly (2007) for five of the meteorological stations (Crosby, Milford Haven, Isle of Portland, Wattisham, and Loftus) and 3-hourly (1975) for the station located furthest offshore (Stevenson).

3.3. Wave Data

For present-day validation of the wave model, time series of significant wave height (H_s) and peak wave period (T_p) were obtained from five CEFAS directional waveriders in regions of varying wave exposure and water depth (Table 2). These data were available for the entire year 2007 at a sampling frequency of 2 h^{-1}. In addition, 3-hourly wave data for 1975 were obtained from a non-directional UK Met Office waverider located further offshore (Stevenson). The locations of the wave buoys are plotted on Figure 1.

4. Modeling

A spectral wave model was used to calculate the present-day and paleo wave climates over the NW European shelf seas. The key model inputs were wind forcing and bathymetry. The wave model was applied at the same spatial resolution as the bathymetry data (1/12°) for time slices from 12 ka BP until present. For the maximum wind speed considered (30 m s^{-1}), the fetch length for a fully developed sea, based on a JONSWAP spectrum [*Carter*, 1982], is 400 km. Hence, although full bathymetric domains were used for the wave simulations, only results > 400 km from the model boundaries were analyzed (Figure 1). Depending on wind speed, waves within this 400 km 'buffer zone' adjacent to the model boundary may be erroneously fetch-limited when waves are propagating from the direction of an open boundary.

4.1. Model Description

SWAN (Simulating WAves Nearshore) is an Eulerian formulation of the discrete wave action balance equation [*Booij et al.*, 1999]. The model is spectrally discrete in frequencies and directions, and the kinematic behavior of the waves is described with the linear theory

of gravity waves. The deep water physics of SWAN are taken from the WAM model [*Komen et al.*, 1994]. The model also includes shallow-water physics, namely bottom friction, refraction and shoaling. SWAN has two modes: stationary and non-stationary. Non-stationary mode is time-dependent, hence the evolution of the wave field can be modeled realistically, using boundary conditions of time-varying wind speed and direction [e.g. *Ris et al.*, 1999; *Neill et al.*, 2007]. This is, however, computationally expensive since a time step much smaller than the wind forcing time step is required for stability. In order to capture the high frequency nature of wind events, wave simulations at high temporal resolution were required for several time slices of the NW European shelf seas. Since the length of simulations was a decade, a more economical method was required. This involved running SWAN in stationary (steady state) mode.

In stationary mode, the evolution of the action density N is governed by the time-independent wave action balance equation [*Booij et al.*, 1999]

$$\frac{\partial}{\partial x}c_x N + \frac{\partial}{\partial y}c_y N + \frac{\partial}{\partial \sigma}c_\sigma N + \frac{\partial}{\partial \theta}c_\theta N = \frac{S}{\sigma} \tag{1}$$

where c_x and c_y are the propagation velocities in the x and y directions, σ is frequency, θ is wave direction and S represents the source terms, i.e. generation, dissipation, and non-linear wave-wave interactions. For this application, the wave energy spectrum at each grid point was divided into 40 frequency components and 45 direction components. The lowest model frequency was 0.05 s^{-1} (period $T = 20$ s, wavelength $L = 625$ m), and the highest frequency resolved by the model was 2 s^{-1} ($T = 0.5$ s, $L = 0.4$ m). The effect of waves at higher frequencies was included in the calculation of the source terms.

For each cell of the model grid, a matrix of significant wave height (H_s), peak wave period (T_p), and the root-mean-square-value of orbital velocity near the bed (U_{rms}) was

produced as a lookup table using a discrete range of wind speeds and directions held constant over the entire model domain. From a consideration of the wind climate over the NW European shelf, a suitable range of discrete wind direction and speed bins was selected as $\theta = 0, 15, \ldots, 345°$ and $W_r = 2, 4, \ldots, 30$ m s^{-1} respectively (i.e. $24 \times 15 = 360$ simulations) [*Neill et al.*, 2008]. The final products of the model (time series of H_s, T_p, and U_{rms}) were derived by applying actual wind data to the lookup tables.

4.2. Model Validation

The wave model was validated with data of H_s and T_p from five wave buoys distributed around the UK coastline (Figure 1, Table 2). Simulations were made for an entire year (2007), using hourly wind data from meteorological stations close to each wave buoy applied to the lookup tables. To determine model performance further offshore, the same comparison was made at a wave buoy located in deeper water (160 m), 3-hourly throughout 1975. The model has captured much of the detail throughout the year in terms of the magnitude and phase of H_s at all six stations (Figure 3). Probability density plots of modeled and observed H_s (Figure 5) demonstrate good model performance at two of the stations (Liverpool Bay and Poole Bay) and reasonable performance at the other four stations. The model performs less satisfactorily when comparing with observed values of T_p (Figure 4). The model often under-predicts T_p (Figure 6), mainly due to an absence of swell waves in the rapid calculation method, since the model has not been nested within a larger area model of the North Atlantic [e.g. *Elliott and Neill*, 2007]. For such a rapid calculation method, it is unrealistic to assume steady wind conditions over a region larger than shelf scale, hence computationally-expensive time-stepping methods would be required to simulate swell waves. However, the model has generally reproduced the

magnitude and character of T_p throughout the year (Figure 4, Figure 6), considering such uncertainties associated with rapid calculation methods.

4.3. Present-Day Benchmark Simulation

ECMWF-ERA-Interim reanalysis 3-hourly synoptic wind data described in section 3.2 were applied to lookup tables calculated for every cell of the shelf model grid. A benchmark simulation was made for the entire 'typical' year 1993 when the annual NAO index was closest to zero (0.12) for the available decade of wind data (Table 1). Outputs at all time steps throughout 1993 were used to calculate the spatial distribution of annual rms and peak H_s, T_p, and τ_w over the NW European shelf seas, considered as the benchmark simulation (Figure 7).

4.4. Paleo Benchmark Simulation

Initially, a steady state SW wind (dominant wind direction over the NW European shelf) of magnitude 22 m s^{-1} (typical gale wind speed) was applied over the entire model domain for every 1 ka time slice from 12 ka BP to present. This identified key periods when there were potentially large transitions in the wave climate over the NW European shelf seas. From these pilot simulations, four paleo time slices were selected, in addition to the present-day time slice described in section 4.3, for more detailed wave modeling: 12, 10, 8, and 6 ka BP. Using the paleobathymetries described in section 3.1, a series of lookup tables were calculated for each paleo time slice, applying the same methodology used for the present-day bathymetry case.

Climate model simulations [*Renssen et al.*, 2007] and proxy data on aeolian sand transport [*Böse*, 1991] indicate that throughout the Holocene, wind directions over NW Europe

were generally similar to present-day wind directions. Therefore, the 3-hourly wind forcing throughout 1993 was applied to each set of lookup tables corresponding to each of the paleo time slices. The resulting paleowave climates for this 'typical' NAO year of wind forcing were calculated (e.g. Figure 8) and contrasted with the present-day bathymetry benchmark simulation. Anomalies in bed shear stress between all paleo simulations and the present-day simulation are presented in Figure 9 (annual rms τ_w) and Figure 10 (annual maximum τ_w). These paleowave model benchmark simulations therefore demonstrate the influence of bathymetry on the resulting wave climate. Sensitivity of the model results to variations in the wind forcing is investigated in section 6.

5. Model Results

Generally, the present-day annual mean wave climate over the NW European shelf seas relates to fetch lengths associated with the predominantly southwesterly winds (Figure 7a,b). Therefore, in the exposed Celtic Sea, the Atlantic seaboards of Ireland and Scotland, and the northern and eastern North Sea, annual rms significant wave heights (H_s) are of order $3-4$ m, in contrast to $1-2$ m in the relatively sheltered Irish Sea, English Channel, and the UK seaboard of the North Sea. The corresponding peak annual H_s for these exposed and sheltered regions are of order $10-15$ m and $5-10$ m, respectively (Figure 7d). Annual rms T_p in exposed and sheltered regions of the shelf seas are typically $7-8$ s and $5-6$ s, respectively (Figure 7b). Peak annual T_p in exposed and sheltered regions are typically $18-19$ s and $13-14$ s, respectively (Figure 7e). Wave height (and hence wave energy) at shelf scale is mainly a function of wind/wave exposure and is largely independent of water depth. However, due to the attenuation of wave orbital velocity with depth, bed shear stress is strongly related to water depth and the

level of exposure. Therefore, present-day annual rms wave-induced bed shear stresses are greatest in the relatively shallow (water depths of order $30-40$ m) regions of the North Sea (Figure 7c), particularly Dogger Bank and the German Bight. In these regions, the modest mean wave orbital motion available at the surface (Figure 7a) has a significant influence on the bed since relatively little net attenuation occurs in such shallow water depths. Annual rms bed shear stress in these regions is therefore relatively high - of order $1-2$ N m^{-2}. In contrast, wave motion is considerably attenuated at the bed in the deeper, but more exposed, Celtic Sea and northern North Sea, leading to low annual rms values of wave-induced bed shear stress - of order $0-0.5$ N m^{-2}. The corresponding peak annual bed shear stress in these shallow and deep regions is of order $5-10$ N m^{-2} and $0-2$ N m^{-2}, respectively.

In contrast to simulations which use the present-day bathymetry, results of the wave model applied to the 12 ka BP bathymetry indicate that annual rms and peak annual significant wave heights were reduced over the remaining 'wet' regions of the shelf seas (Figure 8a,d). This decrease was due to shoaling and the reduction in fetch lengths resulting from changes in relative sea level redefining the position of the coastline. In the Celtic Sea, annual rms wave heights were relatively constant between 12 ka BP and present (Figure 7a, Figure 8a), but in the northern North Sea, annual rms wave heights were about 1 m lower at 12 ka BP. In the case of peak annual wave heights, in contrast to the present-day wave climate, there was a decrease of order $3-4$ m at 12 ka BP in both the Celtic Sea and the northern North Sea (Figure 7d, Figure 8d). However, despite a reduction in wave heights over the shelf seas at 12 ka BP, wave-induced bed shear stresses were considerably higher at 12 ka BP, in contrast to the present-day. Since wave

orbital motion is attenuated with depth, at 12 ka BP there was an overall increase in wave motion at the bed, and hence higher bed shear stress, over this shallower shelf. Annual rms and peak annual bed shear stress at 12 ka BP are plotted in Figure 8c and Figure 8f, respectively, but the contrast between present-day bed shear stress is made clearer in the anomaly plots of Figure 9 and Figure 10. These plots also contain information at intermediate time slices 6, 8, and 10 ka BP. Generally, as sea levels rose over the last 12,000 years, water depth over the shelf seas increased, accompanied by a reduction in wave-induced bed shear stress. Beginning with the 12 ka BP time slice, annual rms bed shear stresses were much higher than present in the Celtic Sea and northwest North Sea (Figure 9d). In contrast, peak annual bed shear stress was significantly increased in most regions of the shelf seas which were 'wet', particularly the Celtic Sea, exposed Atlantic waters of Ireland and Scotland, and the northern North Sea (Figure 10d). At 10 ka BP, annual rms bed shear stresses were considerably higher than present in the central northern North Sea (Figure 9c), whereas peak annual bed shear stress was again significantly increased in most regions of the shelf seas (Figure 10c). At 8 ka BP (Figure 9b), annual rms bed shear stresses over Dogger Bank and in the German Bight were significantly higher than present-day values. Due to shoaling, the peak annual bed shear stresses in these relatively shallow regions remained similar to present-day values at this time slice, whereas peak annual bed shear stress increased in both the northern North Sea and the Celtic Sea (Figure 10b). Other than a slight increase in annual rms bed shear stress over Dogger Bank, the results at 6 ka BP were generally similar to present-day conditions (Figure 9a, Figure 10a), since relatively little change in sea level occurred over the last 6000 years.

6. Sensitivity to Inter-Annual Variability in Wind Forcing

The results discussed in section 5 were based on the 3-hourly synoptic wind forcing for 1993, applied to discrete time slices from 12 ka BP to present. Clearly, paleo wind climates were different to present-day wind climates. However, wind predictions from paleoclimate models [e.g. *Renssen et al.*, 2007] are not available for all our timeslices, at the same high spatial/temporal resolution, for the same duration or validated to the same extent as the ECMWF-ERA-Interim reanalysis data (see PMIP2 database - http://pmip2.lsce.ipsl.fr/pmip2/). Therefore, in order to represent the variability in wind climate over the NW European shelf seas during the last 12 ka, the model was run with ECMWF-ERA-Interim reanalysis years in the decade $1989-1998$. This decade contained considerable variation in the NAO, with annual means ranging from -1.01 (1996) to 1.23 (1990) (Table 1). Thus, while we cannot force the model with observed or modelled wind data from the different time slices, this range of years covers synoptic conditions ranging from generally anticyclonic (more negative NAO), and so characteristically cold and dry, to mostly strong westerlies (positive NAO), and warm and wet. This range of conditions gives an estimate of the sensitivity of the wave heights and bed shear stress to atmospheric forcing, and so enables identification of trends over time due to bathymetric changes rather than atmospheric forcing.

The model results are presented as the annual rms and peak annual H_s (Figure 11) and τ_w (Figure 12), averaged over two regions. The first averaging region (used to calculate Figure 11a,b and Figure 12a,b) used only model cells which remained 'wet' continuously over the last 12,000 years, i.e. the area used to compute these averages was fixed, regardless of time slice. The second averaging region (used to calculate Figure 11c,d and Figure

12c,d) used only model cells with water depth $h < 100$ m at each time slice, i.e. this averaging region varied between time slices. There is significant spread in the results (Figure 11 and Figure 12), reflecting the inter-annual variability in wind forcing, but two trends dominate. Whereas annual rms and peak annual wave heights progressively increased over the NW European shelf seas during the last 12,000 years (Figure 11), wave-induced bed shear stress progressively decreased over the same period (Figure 12). In the region of the shelf seas which were continuously wet over the last 12,000 years, annual rms H_s increased by around 20% over the last 12 ka (Figure 11a) and peak annual H_s increased by around 40% (Figure 11b). In the same region, annual rms τ_w was reduced by almost an order of magnitude from ~ 0.4 N m^{-2} at 12 ka BP to 0.06 N m^{-2} at 0 ka BP (Figure 12a), while peak annual τ_w was reduced from 2 to 0.8 N m^{-2} (Figure 12b). Considering only water depths $h < 100$ m at each time slice, annual rms H_s increased by around 15% over the last 12,000 years (Figure 11c) and peak annual H_s increased by around 30% (Figure 11d). Using the same criteria for the averaging region at each time slice ($h < 100$ m), annual rms τ_w was reduced from around 0.5 to 0.3 N m^{-2} over the last 12,000 years (Figure 12c), while peak annual τ_w was reduced from 3 to 2.6 N m^{-2} (Figure 12d).

7. Discussion

Over the last 12,000 years, annual rms and peak annual significant wave heights (H_s) increased over the NW European shelf seas (Figure 11). This was primarily due to an increase in relative sea levels through the Late-glacial and Holocene redefining the location of the coastline, and hence progressively extending fetch lengths in most regions of the shelf seas. This increase in wave heights is particularly noticeable in the northwestern

North Sea and the Irish Sea (Figure 7a,d and Figure 8a,d). However, regardless of this change in fetch length, peak annual wave heights also increased in many exposed regions such as the Celtic Sea. In the Celtic Sea, southwesterly winds are responsible for the largest waves. Since such waves are not fetch-limited, the increase in peak annual wave height from 12 ka BP to present in this region must be due to changes in relative water depth. For a given wave period T, wavelength L is related to water depth h through the dispersion relationship

$$\sigma^2 = gk \tanh(kh) \tag{2}$$

where $\sigma = 2\pi/T$ is the angular frequency and $k = 2\pi/L$ is the wave number. Hence, wavelength (and therefore wave height) will increase with increasing water depth. Therefore, an increase in relative sea level through the Late-glacial and Holocene corresponds to an increase in peak wave heights in regions where the low-frequency waves are not fetch-limited, such as the Celtic Sea.

Over the last 12,000 years, annual rms and peak annual wave-induced bed shear stress (τ_w) decreased over the NW European shelf seas (Figure 12). This reduction in bed shear stress can largely be explained by increasing water depths through the Late-glacial and Holocene. Wave orbital velocities are at a maximum at the surface and attenuate with depth as a function of wavelength. Since the vertical component of velocity w is zero at the bed, it is the horizontal component of velocity u which is responsible for bed shear stress. The amplitude of u is attenuated with depth as

$$u_0 = \frac{\pi H}{T}\left[\frac{\cosh(k(z+h))}{\sinh(kh)}\right] \tag{3}$$

This calculation at the bed is shown graphically in Figure 13 for a range of H and T, applied to a range of water depths h. The mean depth in the Celtic Sea is shown on the plot at two different time slices: 12 ka and 0 ka BP. In the Celtic Sea, the annual rms value of H_s at 12 ka BP was typically 2.25 m (Figure 11a), corresponding with a value of $u_0 = 0.15$ m s^{-1}, plotted as a filled triangle in Figure 13. At 0 ka BP, annual rms H_s increased to 2.75 m in the Celtic Sea, corresponding with a negligible value of $u_0 = 0.002$ m s^{-1}, plotted as a filled circle in Figure 13. Therefore, despite a 0.5 m increase in annual rms H_s over the last 12,000 years, the amplitude of horizontal particle velocity at the bed was reduced by two orders of magnitude in the Celtic Sea. Since τ_w is a function of u_0^2, bed shear stress in this region will be reduced by several orders of magnitude.

The increase in wave height in the southern North Sea over the last 8000 years is consistent with the findings of other studies [e.g. *Beets et al.*, 1992; *van der Molen and de Swart*, 2001a]. This gives confidence in the results of the present study, which has extended these calculations back to 12 ka BP (Figure 11) and over a much larger geographical area. In terms of wave-effects at the bed, previous model studies of the southern North Sea have demonstrated that the magnitude of wave-induced bed load transport decreased through the Holocene [*van der Molen and de Swart*, 2001a]. In addition, numerical and seismic studies in the Celtic Sea have indicated that tidal and wave erosion at the top of sand banks is at present much weaker than during the early Holocene [*Belderson et al.*, 1986; *Reynaud et al.*, 1999]. Again, these published results are consistent with the findings of the present study (Figure 12) which apply to a larger geographic region.

It was suggested in section 1 that the shelf-scale ratio between wave- and tidal-induced bed shear stress will have varied considerably over the Late-glacial and Holocene due to

changes in water depth. Wave-induced bed shear stress is considerably more sensitive to changes in water depth than tidal-induced bed shear stress. Here we introduce mean tidal-induced stress τ_0 in terms of quadratic bottom drag by using paleotidal model output from *Uehara et al.* [2006] as

$$\tau_0 = \rho C_D \overline{U_{M_2}^2} \tag{4}$$

where $\rho = 1023$ kg m^{-3} is the density of seawater, $C_D = 0.0026$ is the drag coefficient and $\overline{U_{M_2}^2}$ is the square of the M_2 tidal current averaged over a tidal cycle. The instantaneous velocities u and v in an ellipse can be written as

$$u = U_{maj}\cos(\omega t) \quad \text{and} \quad v = U_{min}\sin(\omega t) \tag{5}$$

where u and v are velocity components along major and minor axes of the ellipse, U_{maj} and U_{min} are the semi-major and semi-minor axes of the M_2 tidal current ellipses and ω is the angular frequency. Therefore, the square of the tidal current averaged over a tidal cycle is

$$\begin{aligned} \overline{U^2} &= U_{maj}^2\overline{\cos^2(\omega t)} + U_{min}^2\overline{\sin^2(\omega t)} \\ &= \frac{1}{2}(U_{maj}^2 + U_{min}^2) \end{aligned} \tag{6}$$

Hence, equation 4 can be written as

$$\tau_0 = \frac{1}{2}\rho C_D (U_{maj}^2 + U_{min}^2) \tag{7}$$

By combining values of τ_0 with the results of the present study, variations in the spatial distribution of the ratio τ_w/τ_0 over the Late-glacial and Holocene can be quantified for the NW European shelf seas (Figure 14). It is to be noted that this ratio compares the wave-induced bed shear stress with bed shear stress generated by only the M_2 tidal currents.

In reality, the ratio τ_w/τ_0 will be lower, due to the addition of further tidal constituents. However, at 12 ka BP waves generally dominated bed shear stress in the northwest North Sea (Figure 14e). At present, waves generally dominate over Dogger Bank and the eastern North Sea (Figure 14a). By making use of the two averaging regions described in section 6, shelf-scale variations in mean tidal-induced bed shear stress (τ_0) over the last 12,000 years are plotted, along with variations in the annual rms wave-induced bed shear stress (τ_w) (Figure 15a,c). Over the region of the shelf seas which remained wet continuously over the last 12,000 years, the ratio $\tau_w/\tau_0 \approx 1$ at 12 ka BP (Figure 15b). This ratio reduced over the last 12,000 years in this fixed region to its present-day estimate of $\tau_w/\tau_0 = 0.5$. Since these calculations are for a region which is fixed, regardless of changes in water depth at each time slice, it is also useful to compare the ratio τ_w/τ_0 for only regions of the shelf seas with water depths $h < 100$ m at each time slice. In this case, the ratio τ_w/τ_0 remained close to 1 over the last 12,000 years (Figure 15d). However, there was an anomaly at 8 ka BP when $\tau_w/\tau_0 \approx 1.7$, due to a relatively large reduction in τ_0 at this time slice. This anomaly is also present, but not as prominent, in the fixed averaging region (Figure 15b). The global tidal model of *Uehara et al.* [2006] demonstrates that in the period between the LGM and present, the minimum value of global tidal dissipation rate occurred at 8 ka BP. It is to be noted that mean τ_0 (Figure 15a,c) was smaller than peak τ_w (Figure 12b,d) at all time slices, indicating the larger impact of wave processes than tidal effects during storm events throughout the Late-glacial and Holocene.

Although the trend of decreasing τ_w through the Late-glacial and Holocene is clear (Figure 12), there is considerable spread in the results when considering inter-annual variability in wind forcing (Table 1). In addition, although the range of inter-annual

variability of peak annual τ_w in the fixed averaging region (model cells which were wet continuously from 12 ka BP to present) remained approximately constant over the last 12,000 years (Figure 12b), there was a considerable reduction in the range of inter-annual variability in annual rms τ_w over the last 12,000 years in the same region (Figure 12a). Increased inter-annual variability in annual rms τ_w at 12 ka BP can be explained with reference to the Celtic Sea. For typical water depths in the Celtic Sea at 12 ka BP, the mean annual wave climate corresponds with an amplitude of horizontal particle velocity at the bed $u_0 = 0.15$ m s^{-1} (filled triangle on Figure 13). This has reduced considerably to its present-day value of $u_0 = 0.002$ m s^{-1} (filled circle on Figure 13), despite a 0.5 m increase in annual rms wave height. Since inter-annual variability of annual rms wave heights has been relatively constant over the last 12,000 years (Figure 11), it is clear from Figure 13 that for a fixed range of variability in H_s, variability of u_0 (and hence τ_w) will be considerably greater at $h = 30$ m (representing the 12 ka BP time slice), compared with $h = 100$ m (representing the present-day time slice). This explains the greater inter-annual variability of τ_w at 12 ka BP compared to 0 ka BP on Figure 12a. There is little change in the inter-annual variability of peak annual τ_w over the last 12,000 years (e.g. Figure 12b) since the annual peak at any location is generally due to a single annual 'extreme' event, located towards the right-hand-side of Figure 13, and therefore due to a narrow range of wind/wave conditions.

8. Conclusions

Using the present-day bathymetry of the NW European shelf seas, a wave model was first validated using high resolution data from a series of wave buoys. Applying a decade of 3-hourly wind fields, the model was then applied to a series of paleobathymetries, to

contrast wave climates of the NW European shelf seas for time slices 12, 10, 8, 6, and 0 ka BP. Model results demonstrated that wave heights increased through the Late-glacial and Holocene in regions of the shelf seas which were wet continuously over this time period. This increase in wave height was a consequence of increases in fetch length due to changes in relative sea level redefining the position of the coastline for successive time slices. This increase in wave height was accompanied by a large reduction in the annual rms wave-induced bed shear stress, primarily due to a reduction in the magnitude of wave orbital velocity penetrating to the bed for increasing relative sea level. Comparison of wave model output with results of a previous paleotidal model study over the same study area demonstrated significant changes in the spatial distribution of the ratio of annual rms wave- to tidal-induced bed shear stress over the last 12,000 years. In regions of the shelf seas which remained wet continuously over the last 12,000 years, the annual mean ratio of wave- to (M_2) tidal-induced bed shear stress decreased from 1 (at 12 ka BP) to its present day value of 0.5. Therefore, compared to present-day conditions, waves had a more important contribution to large-scale sediment transport processes in the Celtic Sea and the northwestern North Sea at 12 ka BP.

Acknowledgments. The paleobathymetry data were provided by Kurt Lambeck, Australian National University. The 3-hourly synoptic wind data were provided by the European Centre for Medium-Range Weather Forecasts (ECMWF) and hourly time series of wind data from meteorological stations around the UK provided by the UK Met Office. Wave buoy data were provided by the UK Centre for Environment, Fisheries and Aquaculture Science (CEFAS) and the British Oceanographic Data Centre (BODC). NAO data are publicly available from Tim Osborn, University of East Anglia. The authors would also

like to thank two anonymous reviewers for their constructive comments. James Scourse acknowledges the support of a Royal Society-Leverhulme Trust Senior Research Fellowship. Simon Neill acknowledges the support of the Higher Education Funding Council for Wales and the Welsh Assembly Government.

References

Austin, R. M., Modelling Holocene tides on the NW European continental shelf, *Terra Nova*, *3*, 276–288, 1991.

Barrow, E., and M. Hulme, Describing the surface climate of the British Isles, in *Climates of the British Isles*, edited by M. Hulme and E. Barrow, pp. 33–62, Routledge, London, 1997.

Beets, D. J., L. van der Valk, and M. J. F. Stive, Holocene evolution of the coast of Holland, *Mar. Geol.*, *103*, 423–443, 1992.

Belderson, R. H., R. D. Pingree, and D. K. Griffiths, Low sea-level tidal origin of Celtic Sea sand banks - evidence from numerical modelling of M_2 tidal streams, *Mar. Geol.*, *73*, 99–108, 1986.

Berger, A., M. F. Loutre, and J. Laskar, Stability of the astronomical frequencies over the Earth's history for paleoclimate studies, *Science*, *255*, 560–566, 1992.

Booij, N., R. C. Ris, and L. H. Holthuijsen, A third-generation wave model for coastal regions - 1. model description and validation, *J. Geophys. Res.*, *104*, 7649–7666, 1999.

Böse, M., A palaeoclimatic interpretation of frost-wedge casts and aeolian sand deposits in the lowlands between Rhine and Vistula in the upper Pleniglacial and Late Glacial, *Z. Geomorphol., Suppl. Band 90*, 15–28, 1991.

505 Boulton, G. S., G. D. Smith, A. D. Jones, and J. Newsome, Glacial geology and glaciology
506 of the last mid-latitude ice sheets, *J. Geol. Soc. London*, *142*, 447–474, 1985.
507 Cameron, T. D. J., M. S. Stoker, and D. Long, The history of Quaternary sedimentation
508 in the UK sector of the North Sea Basin, *J. Geol. Soc. London*, *144*, 43–58, 1987.
509 Carr, S. J., R. Holmes, J. J. M. van der Meer, and J. Rose, The Last Glacial Maximum
510 in the North Sea Basin: micromorphological evidence of extensive glaciation, *J. Quat.*
511 *Sci.*, *21*, 131–153, 2006.
512 Carter, D. J. T., Prediction of wave height and period for a constant wind velocity using
513 the JONSWAP results, *Ocean Eng.*, *9*, 17–33, 1982.
514 Draper, L., Wave climatology of the U.K. continental shelf, in *The north-west European*
515 *shelf seas: the sea bed and the sea in motion. II. Physical and chemical oceanography,*
516 *and physical resources*, edited by F. T. Banner, M. B. Collins, and K. S. Massie, pp.
517 353–368, Elsevier, 1980.
518 Elliott, A. J., and S. P. Neill, Simulating storm waves in the Irish Sea, *Proceedings of the*
519 *Institution of Civil Engineers - Maritime Engineering*, *160*, 57–64, 2007.
520 Hinton, A. C., Holocene tides of The Wash, U.K.: the influence of water-depth and
521 coastline-shape changes on the record of sea-level change, *Mar. Geol.*, *124*, 87–111,
522 1995.
523 Hinton, A. C., Tides in the northeast Atlantic: considerations for modelling water depth
524 changes, *Quat. Sci. Rev.*, *15*, 873–894, 1996.
525 Hurrell, J. W., and H. van Loon, Decadal variations in climate associated with the north
526 Atlantic oscillation, *Clim. Change*, *36*, 301–326, 1997.

Komen, G. J., L. Cavaleri, M. Donelan, K. Hasselmann, S. Hasselmann, and P. A. E. M. Janssen, *Dynamics and Modelling of Ocean Waves*, Cambridge University Press, 1994.

Lambeck, K., Late Devensian and Holocene shorelines of the British Isles and North Sea from models of glacio-hydro-isostatic rebound, *J. Geol. Soc. London*, *152*, 437–448, 1995.

Lambeck, K., and J. Chappell, Sea level change through the last glacial cycle, *Science*, *292*, 679–686, 2001.

Lambeck, K., and A. Purcell, Sea-level change in the Irish Sea since the Last Glacial Maximum: constraints from isostatic modelling, *J. Quat. Sci.*, *16*, 497–506, 2001.

Lambeck, K., A. Purcell, P. Johnston, M. Nakada, and Y. Yokoyama, Water-load definition in the glacio-hydro-isostatic sea-level equation, *Quat. Sci. Rev.*, *22*, 309–318, 2003.

Milne, G. A., J. X. Mitrovica, and D. P. Schrag, Estimating past continental ice volume from sea-level data, *Quat. Sci. Rev.*, *21*, 361–376, 2002.

Mitrovica, J. X., M. E. Tamisea, J. L. Davis, and G. A. Milne, Recent mass balance of polar ice sheets inferred from patterns of global sea-level change, *Nature*, *409*, 1026–1029, 2001.

Neill, S. P., M. R. Hashemi, and A. J. Elliott, An enhanced depth-averaged tidal model for morphological studies in the presence of rotary currents, *Cont. Shelf Res.*, *27*, 82–102, 2007.

Neill, S. P., A. J. Elliott, and M. R. Hashemi, A model of inter-annual variability in beach levels, *Cont. Shelf Res.*, *28*, 1769–1781, 2008.

549 Newell, N. D., Recent terraces of tropical limestone shores, *Z. Geomorphol.*, *Suppl. Band*
550 *3*, 87–106, 1961.

551 Ogston, A. S., and R. W. Sternberg, Sediment-transport events on the northern California
552 continental shelf, *Mar. Geol.*, *154*, 69–82, 1999.

553 Palutikof, J., T. Holt, and A. Skellern, Wind: resources and hazard, in *Climates of the*
554 *British Isles*, edited by M. Hulme and E. Barrow, pp. 220–242, Routledge, London,
555 1997.

556 Peltier, W. R., Ice-age paleotopography, *Science*, *265*, 195–201, 1994.

557 Peltier, W. R., On eustatic sea level history: Last Glacial Maximum to Holocene, *Quat.*
558 *Sci. Rev.*, *21*, 377–396, 2002.

559 Pingree, R. D., and D. K. Griffiths, Sand transport paths around the British Isles resulting
560 from the M_2 and M_4 tidal interactions, *J. Mar. Biol. Assoc. U.K.*, *59*, 497–513, 1979.

561 Renssen, H., C. Kasse, J. Vandenberghe, and S. J. Lorenz, Weichselian Late Pleniglacial
562 surface winds over northwest and central Europe: a model–data comparison, *J. Quat.*
563 *Sci.*, *22*, 281–293, 2007.

564 Reynaud, J.-Y., B. Tessier, S. Berné, H. Chamley, and M. Debatist, Tide and wave
565 dynamics on a sand bank from the deep shelf of the Western Channel approaches,
566 *Mar. Geol.*, *161*, 339–359, 1999.

567 Rippeth, T. P., J. D. Scourse, K. Uehara, and S. McKeown, Impact of sea-level rise
568 over the last deglacial transition on the strength of the continental shelf CO_2 pump,
569 *Geophys. Res. Lett.*, *35*, L24,604, 2008.

570 Ris, R. C., L. H. Holthuijsen, and N. Booij, A third-generation wave model for coastal
571 regions - 2. verification, *J. Geophys. Res.*, *104*, 7667–7681, 1999.

572 Scourse, J. D., K. Uehara, and A. Wainwright, Celtic Sea linear tidal sand ridges, the
573 Irish Sea Ice Stream and the Fleuve Manche: palaeotidal modelling of a transitional
574 passive margin depositional system, *Mar. Geol.*, *259*, 102–111, 2009.
575 Simmons, A., S. Uppala, D. Dee, and S. Kobayashi, ERA-Interim: new ECMWF re-
576 analysis products from 1989 onwards, *ECMWF Newsletter*, *110*, 25–35, 2006.
577 Uehara, K., J. D. Scourse, K. J. Horsburgh, K. Lambeck, and A. P. Purcell, Tidal evolution
578 of the northwest European shelf seas from the Last Glacial Maximum to the present,
579 *J. Geophys. Res.*, *111*, C09,025, 2006.
580 van der Molen, J., The influence of tides, wind and waves on the net sand transport in
581 the North Sea, *Cont. Shelf Res.*, *22*, 2739–2762, 2002.
582 van der Molen, J., and H. E. de Swart, Holocene wave conditions and wave-induced sand
583 transport in the southern North Sea, *Cont. Shelf Res.*, *21*, 1723–1749, 2001a.
584 van der Molen, J., and H. E. de Swart, Holocene tidal conditions and tide-induced sand
585 transport in the southern North Sea, *J. Geophys. Res.*, *106*, 9339–9362, 2001b.
586 Vincent, C. E., A. Stolk, and C. F. C. Porter, Sand suspension and transport on the
587 Middelkerke Bank (southern North Sea) by storms and tidal currents, *Mar. Geol.*, *150*,
588 113–129, 1998.

TABLE CAPTIONS

589 **Table 1.** Annual North Atlantic Oscillation (NAO) index, 1989-1998.

590 **Table 2.** Details of wave buoys and corresponding meteorological stations used for model vali-
591 dation. Validation year was 2007 for all stations, except for Stevenson (1975).

FIGURE CAPTIONS

Figure 1. Bathymetry and coastline of present-day model domain. The dashed line, drawn at a distance of 400 km from the model boundary, represents the fetch length for a fully developed sea, based on the maximum modeled wind speed (30 m s^{-1} - violent storm) and a JONSWAP spectrum. Since the model is not nested within a larger area wave model, model results outside this dashed line were discarded. Asterisks show locations of six wave buoys (labeled) used for model validation: LB=Liverpool Bay, SW=Scarweather, PB=Poole Bay, WG=West Gabbard, TT=Tyne/Tees, and ST=Stevenson. Contours are water depth in meters, relative to mean sea level.

Figure 2. Paleobathymetries for selected time slices. Contours are water depth in meters, relative to mean sea level. Grey shading represents land at each time slice. For reference, thick solid line shows position of present-day coastline. (a) 6 ka BP, (b) 8 ka BP, (c) 10 ka BP, and (d) 12 ka BP.

Figure 3. Agreement between H_s measured at six wave buoys and H_s modeled by SWAN for one year of simulation. The same year of simulation (2007) was used for all validation stations except for Stevenson (1975). Details of the wave buoys are given in Table 2 and locations plotted in Figure 1. (a) Liverpool Bay, (b) Scarweather, (c) Poole Bay, (d) West Gabbard, (e) Tyne/Tees, and (f) Stevenson.

Figure 4. As in Figure 3, but for T_p.

Figure 5. Agreement between modeled and observed H_s shown as probability density plots.

Note that the in situ data for Stevenson is at coarser temporal resolution (3-hourly), and wind direction and magnitude are recorded in discrete intervals of 10° and 0.5 m s^{-1}, respectively; hence the change in resolution and horizontal banding in (f). Also shown is the equality line (dashed) at 45°. Color scale is percentage probability. (a) Liverpool Bay, (b) Scarweather, (c) Poole Bay, (d) West Gabbard, (e) Tyne/Tees, and (f) Stevenson.

Figure 6. As in Figure 5, but for T_p.

Figure 7. Annual (1993) rms and peak annual H_s, T_p and τ_w calculated at each model cell for present-day simulation using spatially-varying 3-hourly wind fields. (a) annual rms H_s, (b) annual rms T_p, (c) annual rms τ_w, (d) peak annual H_s, (e) peak annual T_p, and (f) peak annual τ_w.

Figure 8. Annual rms and peak annual H_s, T_p and τ_w calculated at each model cell for 12 ka BP time slice using spatially-varying 3-hourly wind fields for 1993. (a) annual rms H_s, (b) annual rms T_p, (c) annual rms τ_w, (d) peak annual H_s, (e) peak annual T_p, and (f) peak annual τ_w.

Figure 9. Anomaly in annual rms τ_w between paleo and present-day bathymetry simulations using 1993 wind data. (a) 6 ka BP, (b) 8 ka BP, (c) 10 ka BP, and (d) 12 ka BP.

Figure 10. As in Figure 9, but for peak annual τ_w.

Figure 11. Variation in spatially-averaged annual rms and peak annual H_s for modeled time slices from 12 ka BP until present. In (a) and (b), the region used for averaging is fixed, using only model cells which remained 'wet' continuously from 12 ka BP to present, and hence does not vary in size for averaging applied to each time slice. In (c) and (d), values are averaged over only

model cells with water depth $h < 100$ m, and hence the averaging region varies between time slices. The solid line indicates the results averaged for all years of wind forcing (1989 – 1998) and grey shading indicates the range of variability within this decade of wind forcing. (a) annual rms H_s (fixed area), (b) peak annual H_s (fixed area), (c) annual rms H_s ($h < 100$ m), and (d) peak annual H_s ($h < 100$ m).

Figure 12. As in Figure 11, but for annual rms and peak annual τ_w. (a) annual rms τ_w (fixed area), (b) peak annual τ_w (fixed area), (c) annual rms τ_w ($h < 100$ m), and (d) peak annual τ_w ($h < 100$ m).

Figure 13. Contoured amplitude of horizontal particle velocity u_0 (m s^{-1}) close to the bed for a range of water depths and wave conditions, calculated using equation 3. Horizontal dashed lines indicate mean water depths in the Celtic Sea at 12 ka and 0 ka BP. Where these lines intersect with vertical dashed lines indicates values of u_0 associated with mean annual wave conditions in the Celtic Sea at 12 ka BP (filled triangle) and 0 ka BP (filled circle).

Figure 14. Spatial distribution of annual mean ratio τ_w/τ_0 for present-day and paleo simulations forced with 1993 wind data. (a) 0 ka BP, (b) 6 ka BP, (c) 8 ka BP, (d) 10 ka BP, and (e) 12 ka BP.

Figure 15. Comparison between annual rms wave- and tidal-induced bed shear stress for modeled time slices from 12 ka BP until present. In (a) and (b), the region used for averaging is fixed, using only model cells which remained 'wet' continuously from 12 ka BP to present, and hence does not vary in size for averaging applied to each time slice. In (c) and (d), values are averaged over only model cells with water depth $h < 100$ m, and hence the averaging region

varies between time slices. In (b) and (d), the solid line indicates the mean ratio τ_w/τ_0 for all years of wind forcing ($1989 - 1998$), and grey shading indicates the range of variability within this decade of wind forcing. (a) Annual rms τ_w and τ_0 (fixed area), (b) annual ratio τ_w/τ_0 (fixed area), (c) annual rms τ_w and τ_0 ($h < 100$ m), and (d) annual ratio τ_w/τ_0 ($h < 100$ m).

Year	NAO index
1989	0.57
1990	1.23
1991	0.34
1992	1.11
1993	0.12
1994	0.51
1995	-0.61
1996	-1.01
1997	-0.18
1998	0.25

Name of wave buoy	Latitude	Longitude	Water depth (m)	Corresponding Met. station
Liverpool Bay	53°32′.05N	03°21′.20W	22	Crosby
Scarweather	51°26′.00N	03°56′.00W	30	Milford Haven
Poole Bay	50°38′.11N	01°43′.03W	26	Isle of Portland
West Gabbard	51°58′.80N	02°04′.76E	34	Wattisham
Tyne/Tees	54°55′.10N	00°44′.85W	65	Loftus
Stevenson	61°20′.00N	00°00′.00E	160	Stevenson

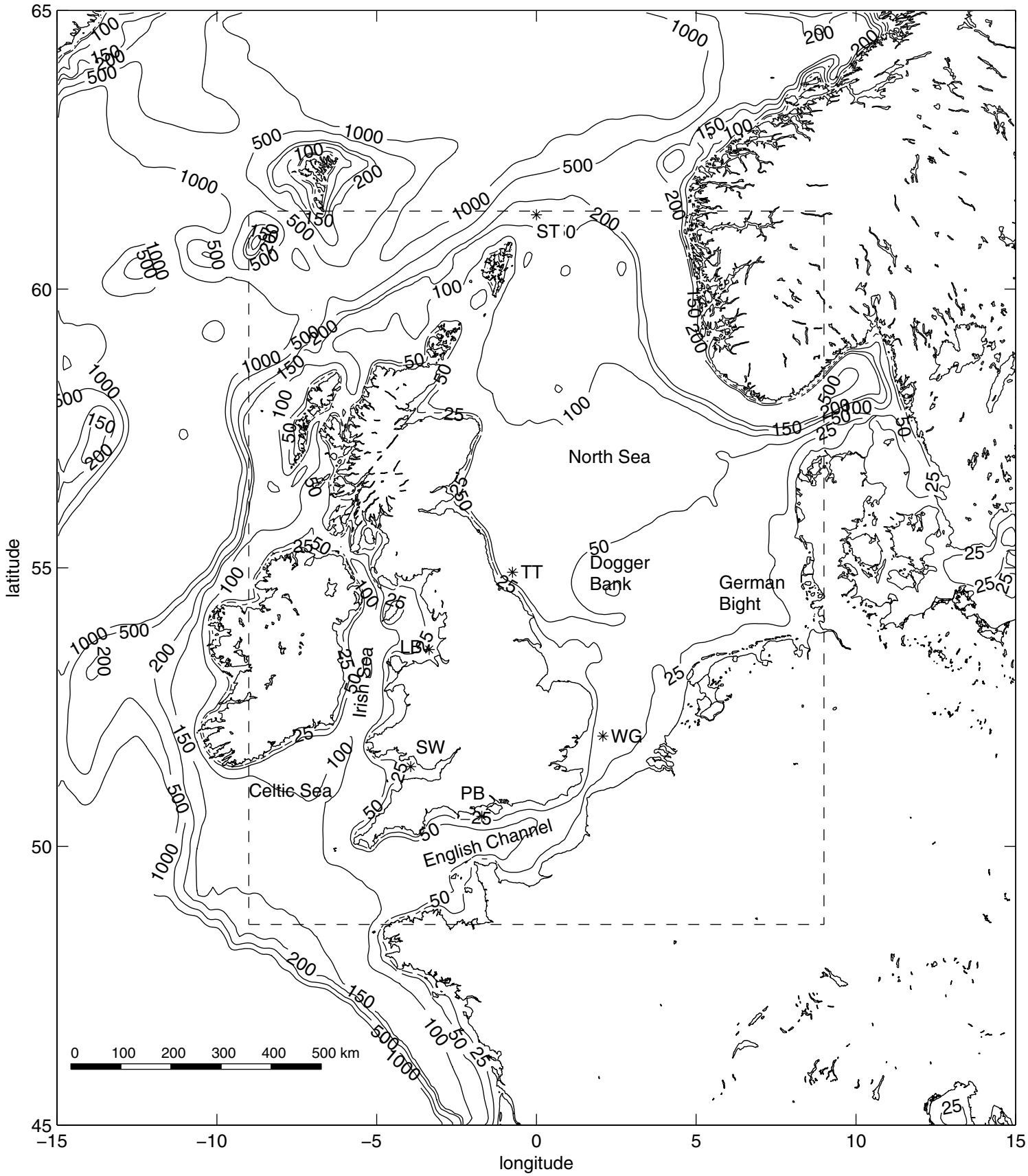
ST 0
TT
WG
LB
SW
PB
North Sea
Dogger Bank
German Bight
Irish Sea
Celtic Sea
English Channel
0 100 200 300 400 500 km
latitude
longitude
65
60
55
50
45
−15
−10
−5
0
5
10
15

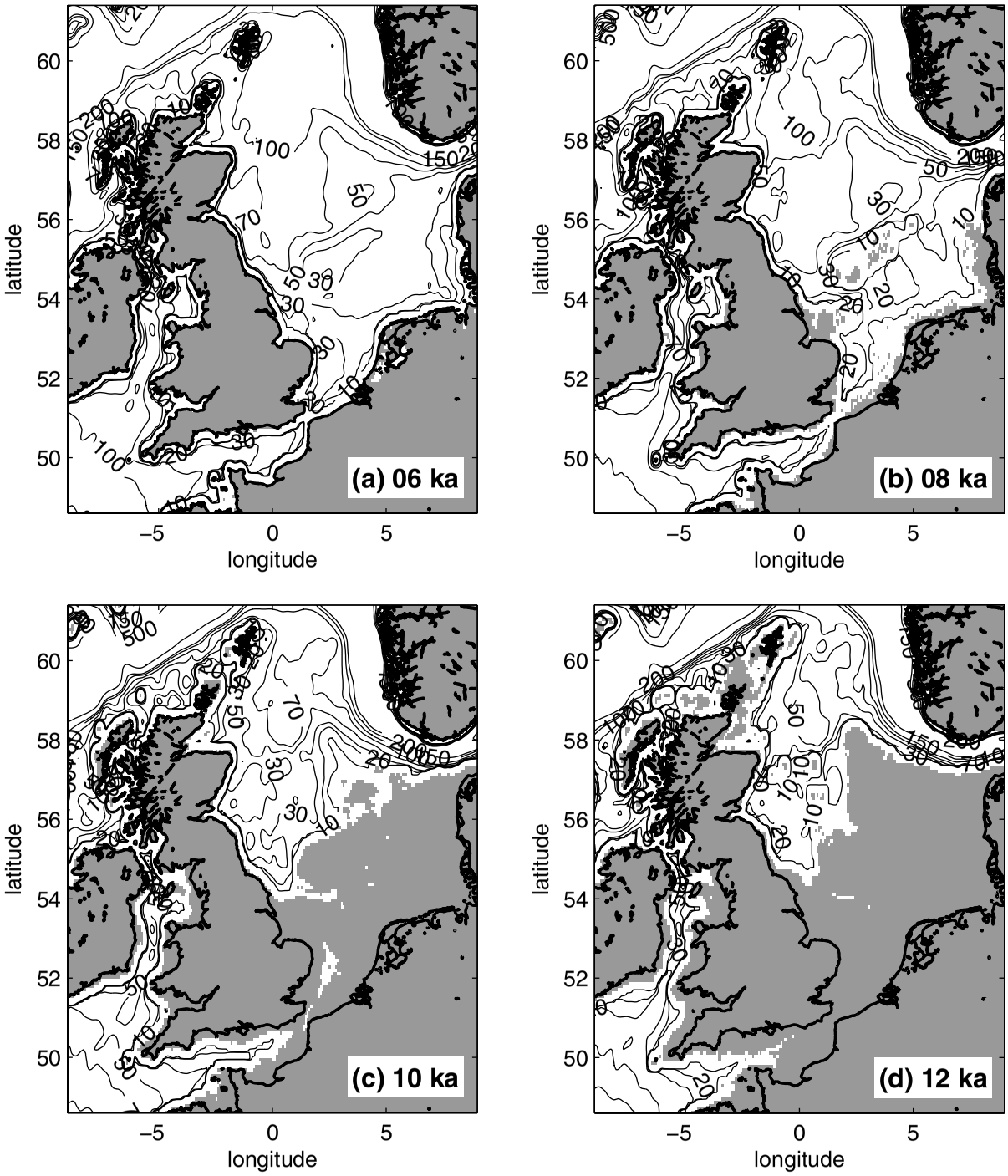
(a) 06 ka
(b) 08 ka
(c) 10 ka
(d) 12 ka
latitude
longitude
60
58
56
54
52
50
−5
0
5

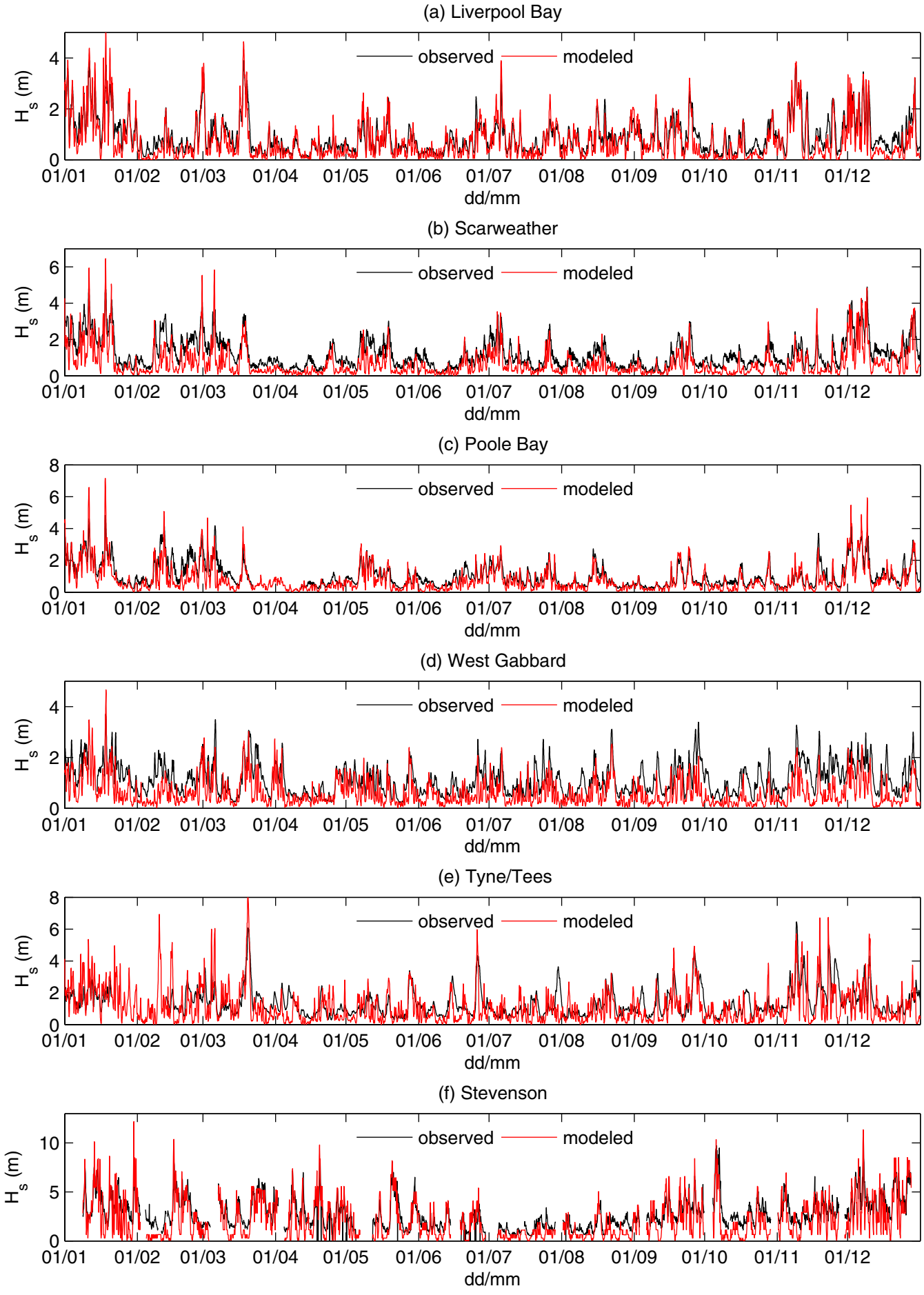
(a) Liverpool Bay
observed
modeled
H_s (m)
0
2
4
01/01
01/02
01/03
01/04
01/05
01/06
01/07
01/08
01/09
01/10
01/11
01/12
dd/mm
(b) Scarweather
observed
modeled
H_s (m)
0
2
4
6
01/01
01/02
01/03
01/04
01/05
01/06
01/07
01/08
01/09
01/10
01/11
01/12
dd/mm
(c) Poole Bay
observed
modeled
H_s (m)
0
2
4
6
8
01/01
01/02
01/03
01/04
01/05
01/06
01/07
01/08
01/09
01/10
01/11
01/12
dd/mm
(d) West Gabbard
observed
modeled
H_s (m)
0
2
4
01/01
01/02
01/03
01/04
01/05
01/06
01/07
01/08
01/09
01/10
01/11
01/12
dd/mm
(e) Tyne/Tees
observed
modeled
H_s (m)
0
2
4
6
8
01/01
01/02
01/03
01/04
01/05
01/06
01/07
01/08
01/09
01/10
01/11
01/12
dd/mm
(f) Stevenson
observed
modeled
H_s (m)
0
5
10
01/01
01/02
01/03
01/04
01/05
01/06
01/07
01/08
01/09
01/10
01/11
01/12
dd/mm

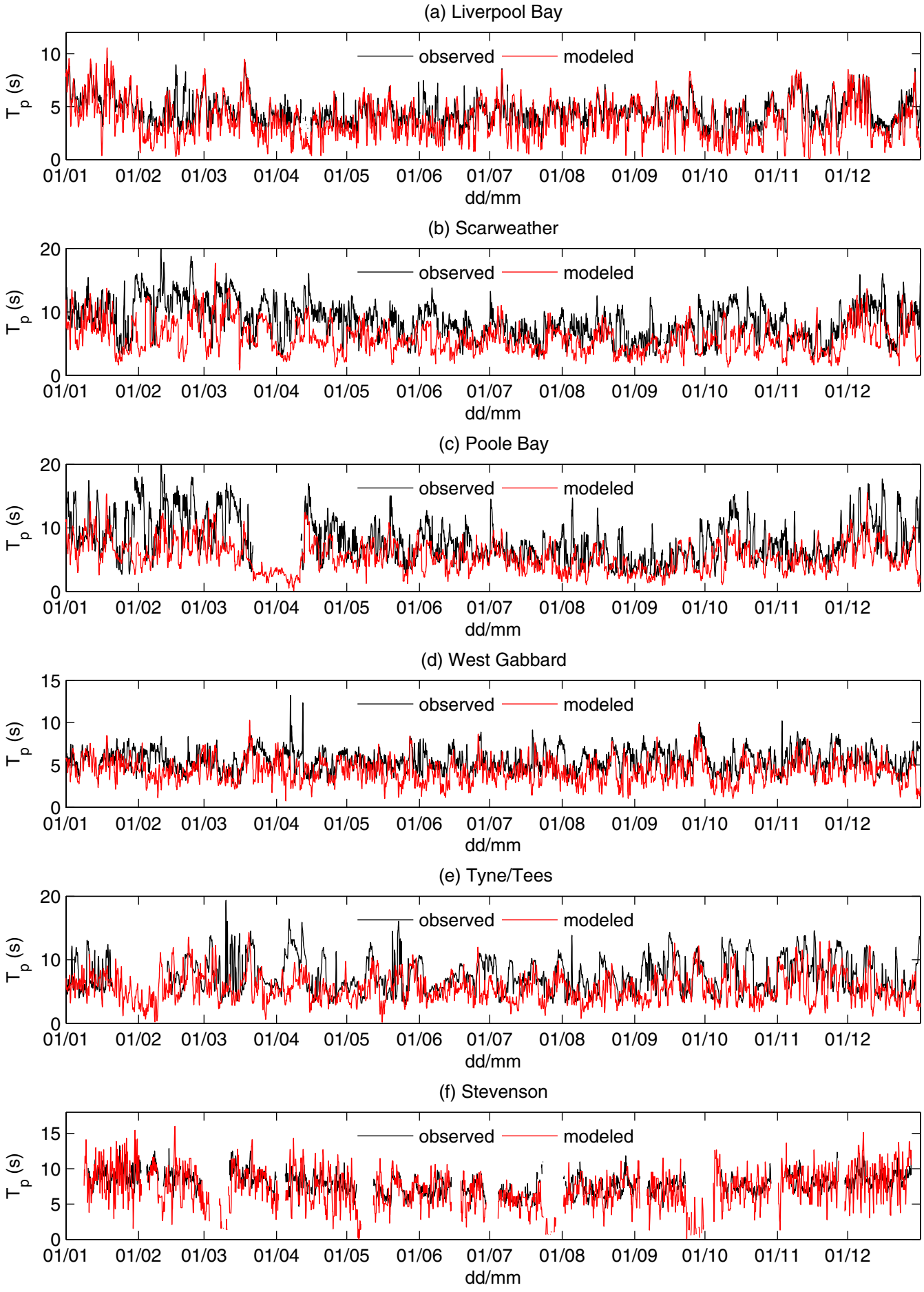
(a) Liverpool Bay
observed
modeled
T_p (s)
0
5
10
01/01
01/02
01/03
01/04
01/05
01/06
01/07
01/08
01/09
01/10
01/11
01/12
dd/mm
(b) Scarweather
observed
modeled
T_p (s)
0
10
20
01/01
01/02
01/03
01/04
01/05
01/06
01/07
01/08
01/09
01/10
01/11
01/12
dd/mm
(c) Poole Bay
observed
modeled
T_p (s)
0
10
20
01/01
01/02
01/03
01/04
01/05
01/06
01/07
01/08
01/09
01/10
01/11
01/12
dd/mm
(d) West Gabbard
observed
modeled
T_p (s)
0
5
10
15
01/01
01/02
01/03
01/04
01/05
01/06
01/07
01/08
01/09
01/10
01/11
01/12
dd/mm
(e) Tyne/Tees
observed
modeled
T_p (s)
0
10
20
01/01
01/02
01/03
01/04
01/05
01/06
01/07
01/08
01/09
01/10
01/11
01/12
dd/mm
(f) Stevenson
observed
modeled
T_p (s)
0
5
10
15
01/01
01/02
01/03
01/04
01/05
01/06
01/07
01/08
01/09
01/10
01/11
01/12
dd/mm

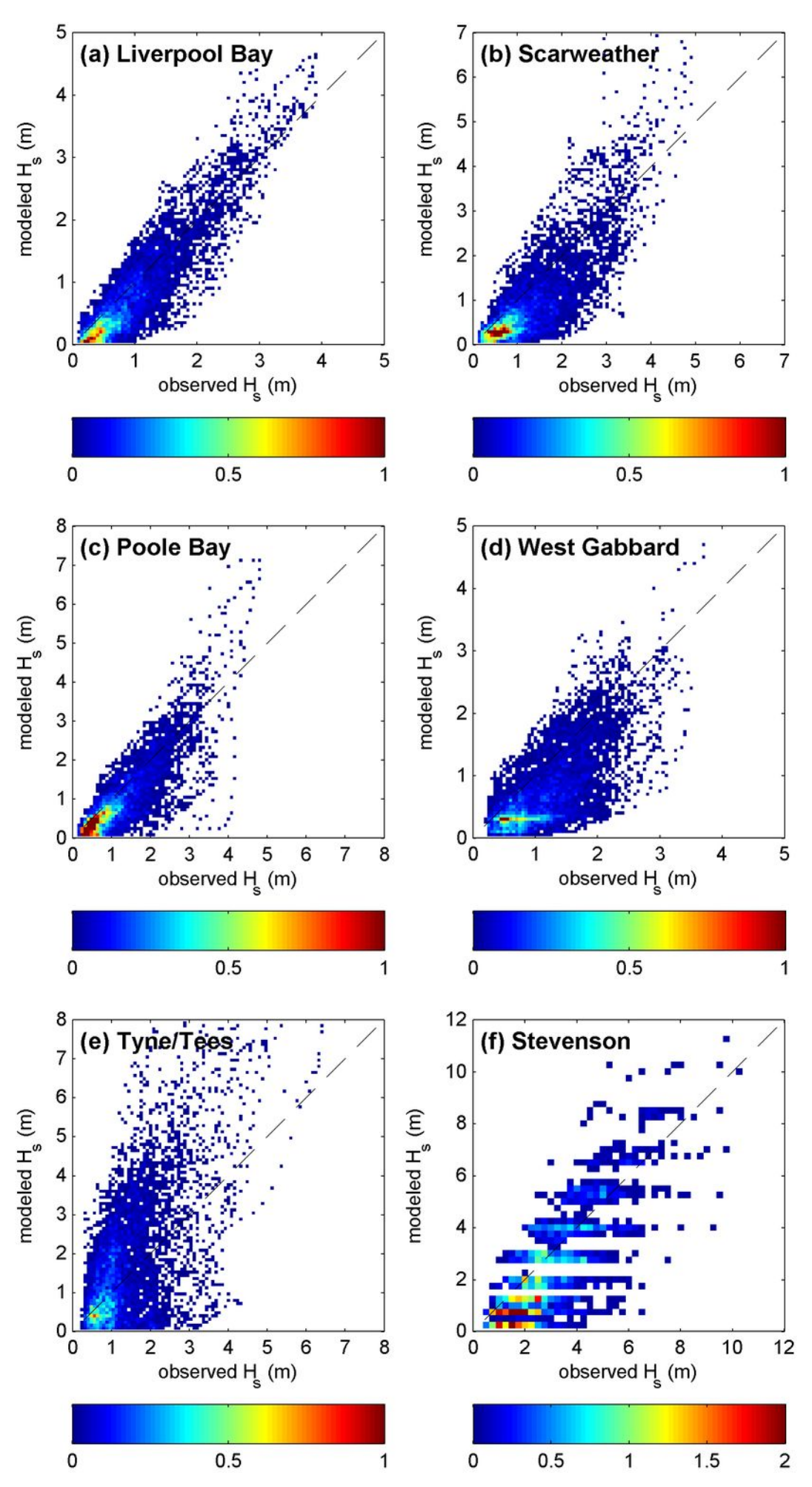
(a) Liverpool Bay
(b) Scarweather
(c) Poole Bay
(d) West Gabbard
(e) Tyne/Tees
(f) Stevenson
modeled H_s (m)
observed H_s (m)

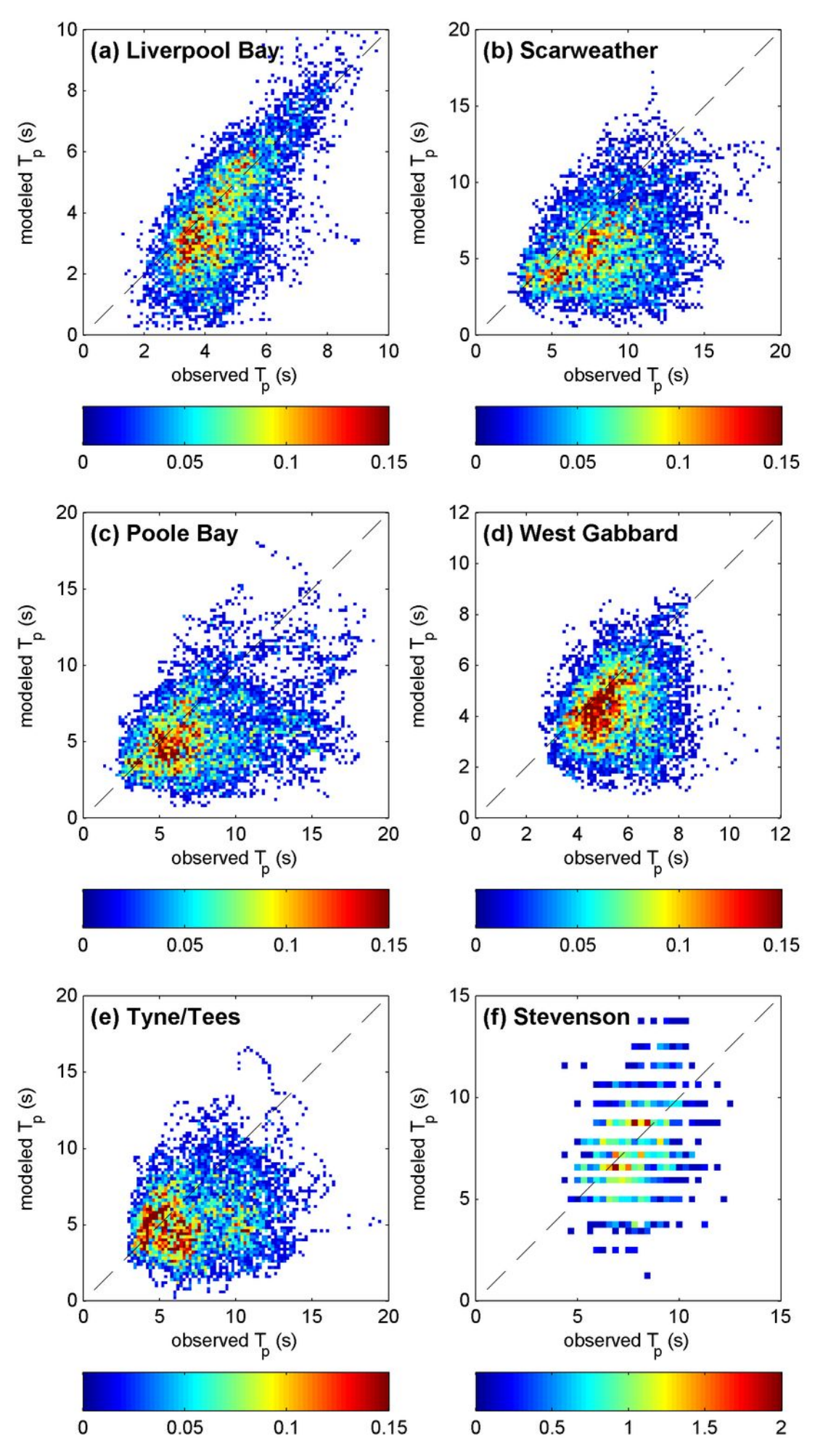
(a) Liverpool Bay
(b) Scarweather
(c) Poole Bay
(d) West Gabbard
(e) Tyne/Tees
(f) Stevenson
modeled T_p (s)
observed T_p (s)
0
0.05
0.1
0.15
0.5
1
1.5
2

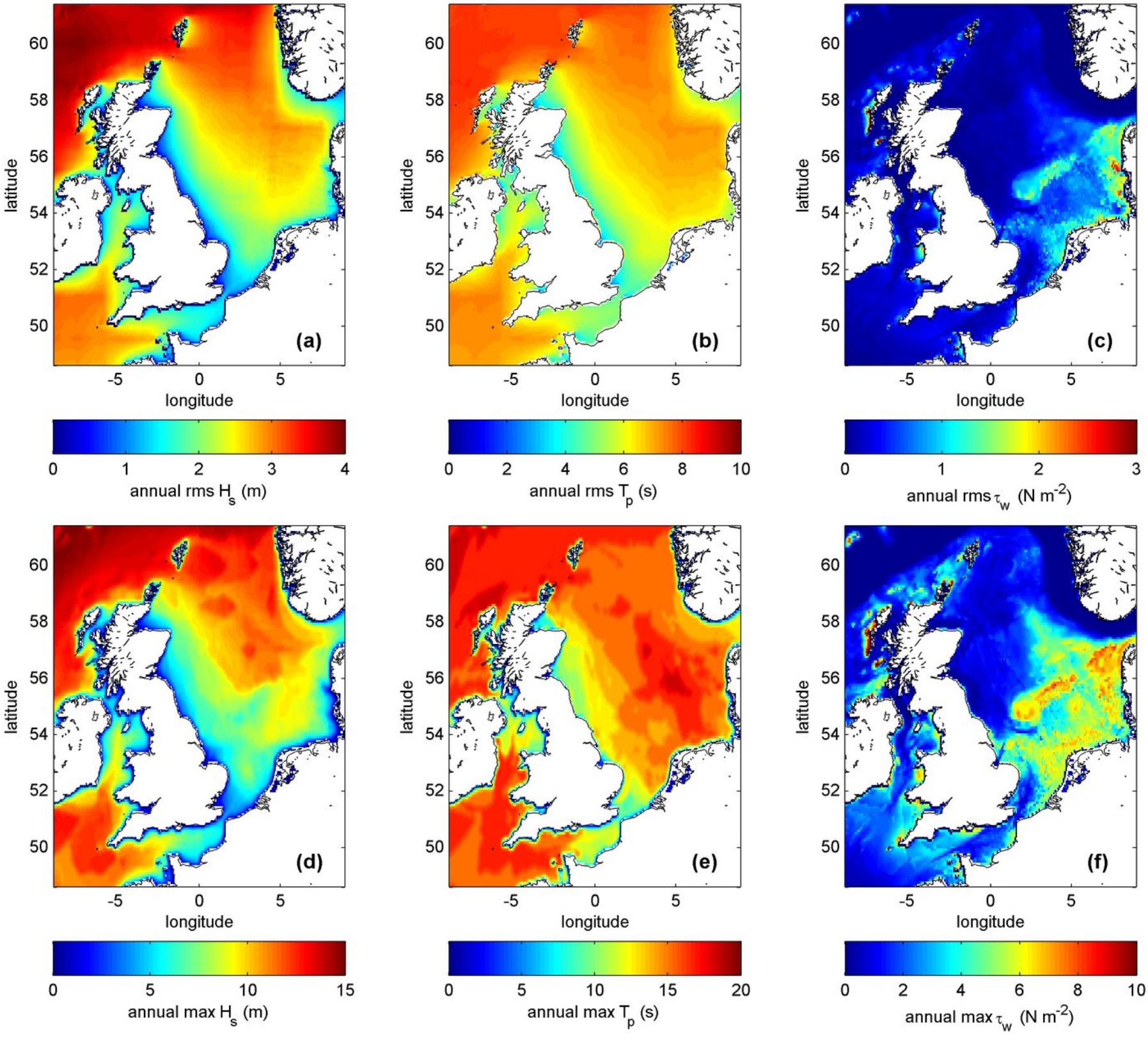
(a)
(b)
(c)
(d)
(e)
(f)
latitude
longitude
60
58
56
54
52
50
-5
0
5
0
1
2
3
4
annual rms H_s (m)
0
2
4
6
8
10
annual rms T_p (s)
0
1
2
3
annual rms τ_w (N m^{-2})
0
5
10
15
annual max H_s (m)
0
5
10
15
20
annual max T_p (s)
0
2
4
6
8
10
annual max τ_w (N m^{-2})

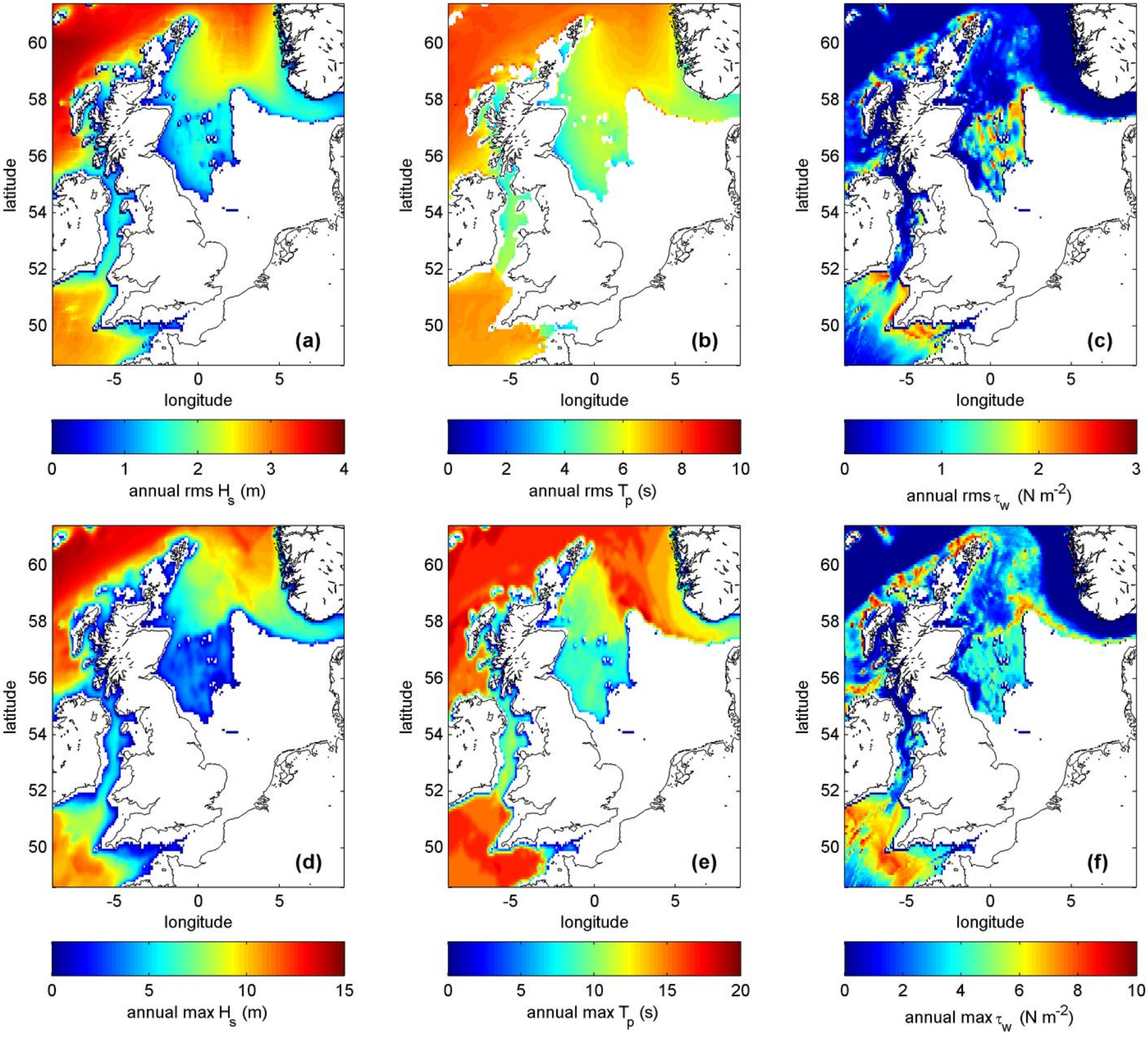
(a)
(b)
(c)
(d)
(e)
(f)
latitude
longitude
60
58
56
54
52
50
-5
0
5
0
1
2
3
4
annual rms H_s (m)
0
2
4
6
8
10
annual rms T_p (s)
0
1
2
3
annual rms τ_w (N m^{-2})
0
5
10
15
annual max H_s (m)
0
5
10
15
20
annual max T_p (s)
0
2
4
6
8
10
annual max τ_w (N m^{-2})

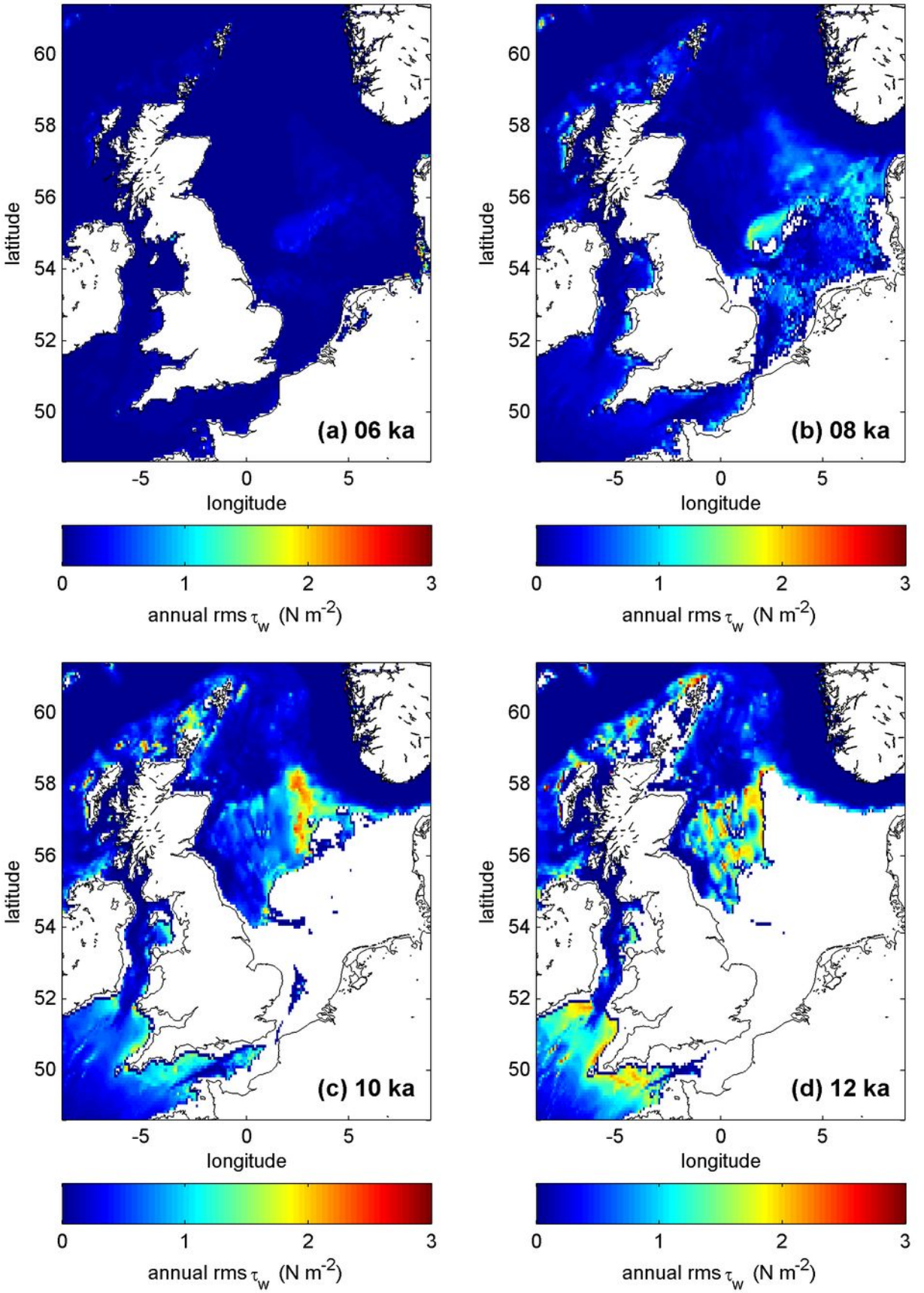
(a) 06 ka
(b) 08 ka
(c) 10 ka
(d) 12 ka
latitude
longitude
60
58
56
54
52
50
-5
0
5
0
1
2
3
annual rms τ_w (N m^{-2})

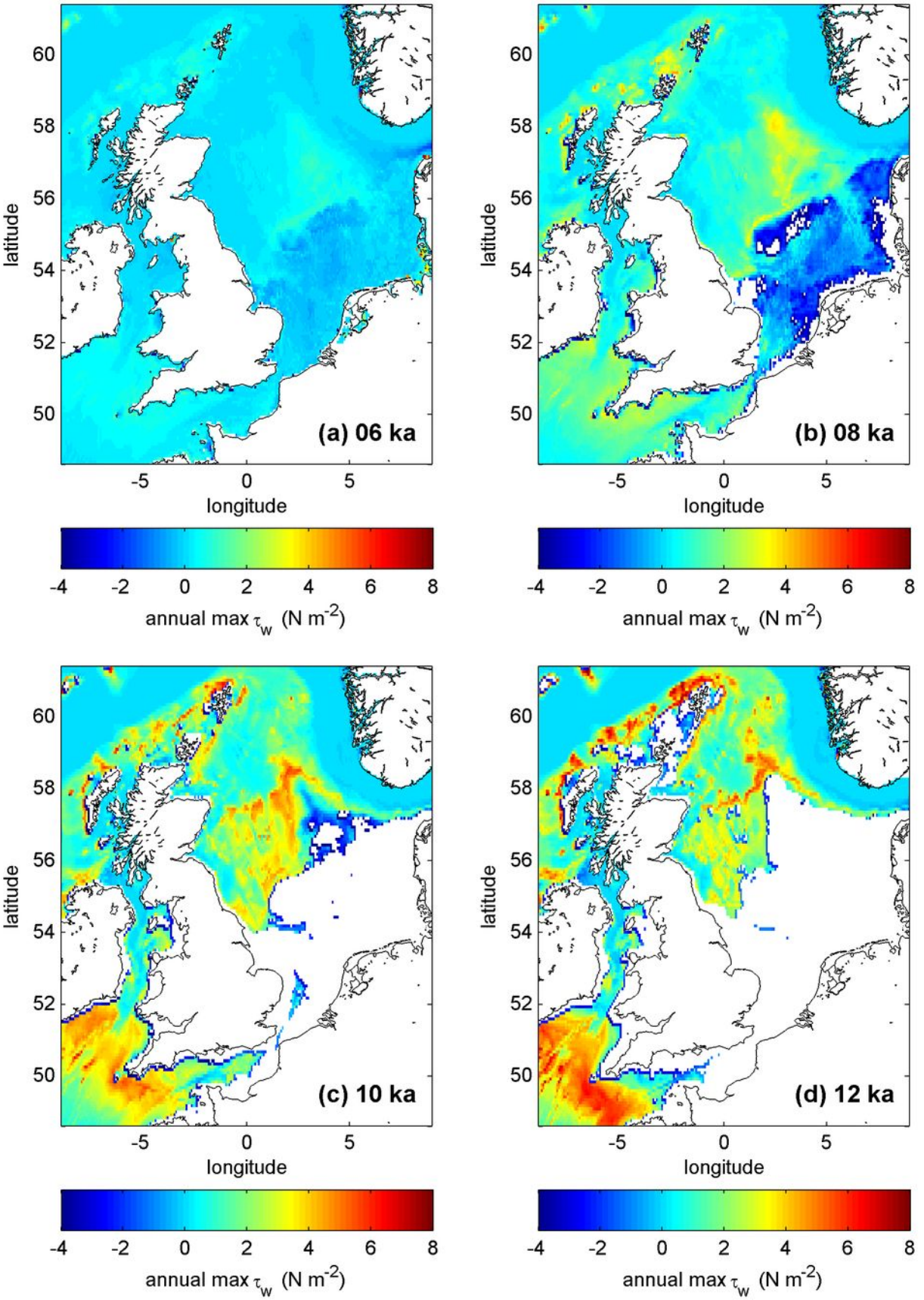
(a) 06 ka
(b) 08 ka
(c) 10 ka
(d) 12 ka
latitude
longitude
60
58
56
54
52
50
-5
0
5
-4
-2
0
2
4
6
8
annual max τ_w (N m^{-2})

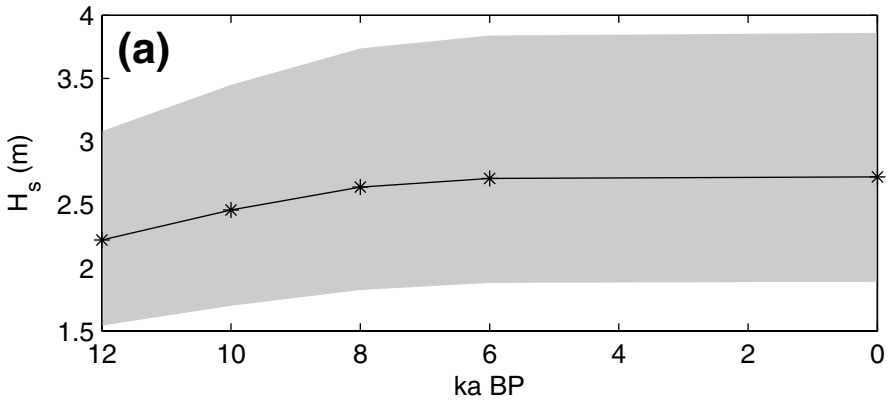
(a)
4
3.5
3
2.5
2
1.5
H_s (m)
12
10
8
6
4
2
0
ka BP

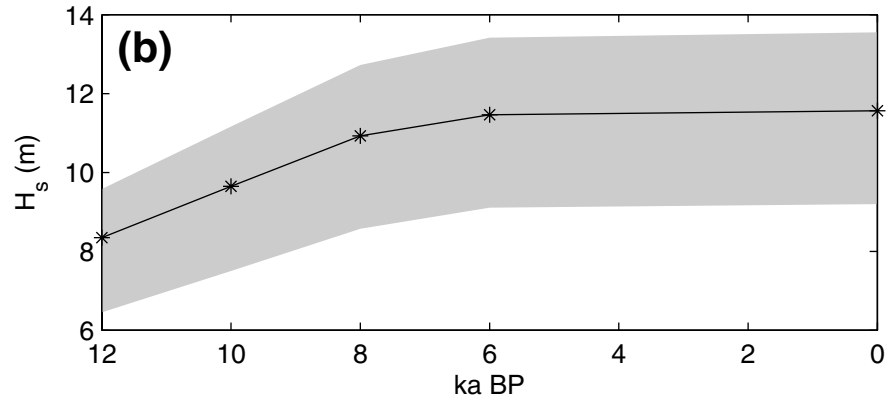
(b)
14
12
10
8
6
H_s (m)
12
10
8
6
4
2
0
ka BP

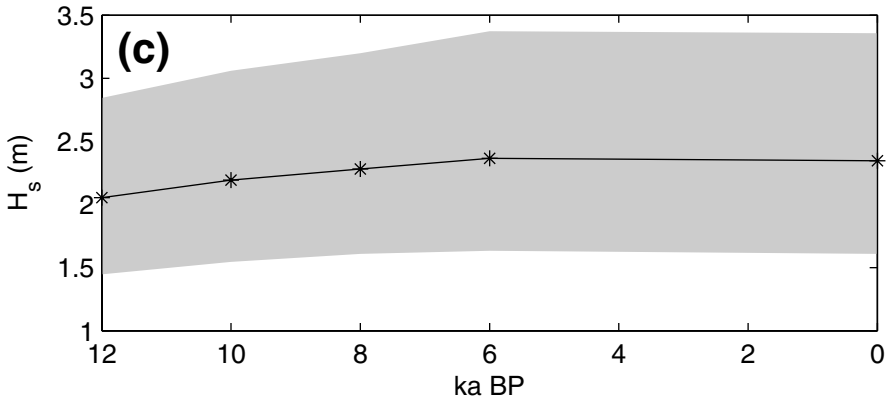
(c)
3.5
3
2.5
2
1.5
1
H_s (m)
12
10
8
6
4
2
0
ka BP

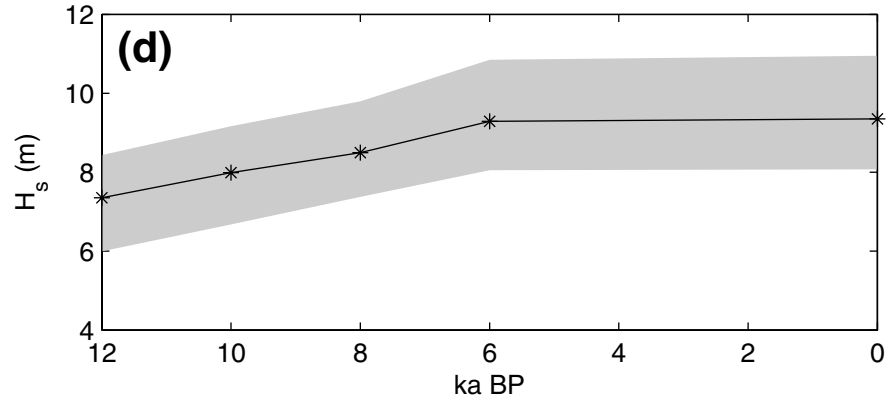
(d)
12
10
8
6
4
H_s (m)
12
10
8
6
4
2
0
ka BP

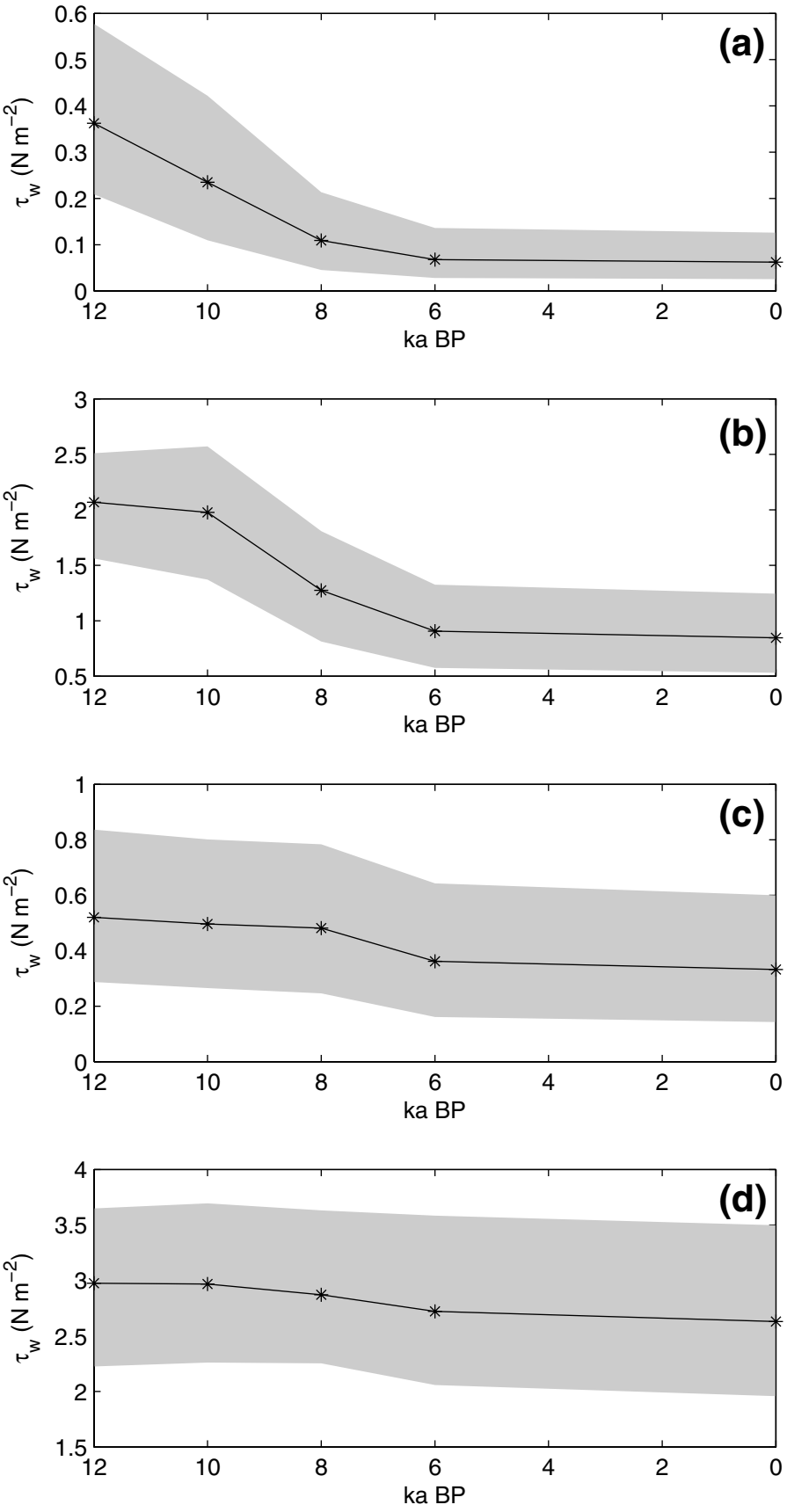
(a)
(b)
(c)
(d)
τ_w (N m^{-2})
ka BP
12
10
8
6
4
2
0

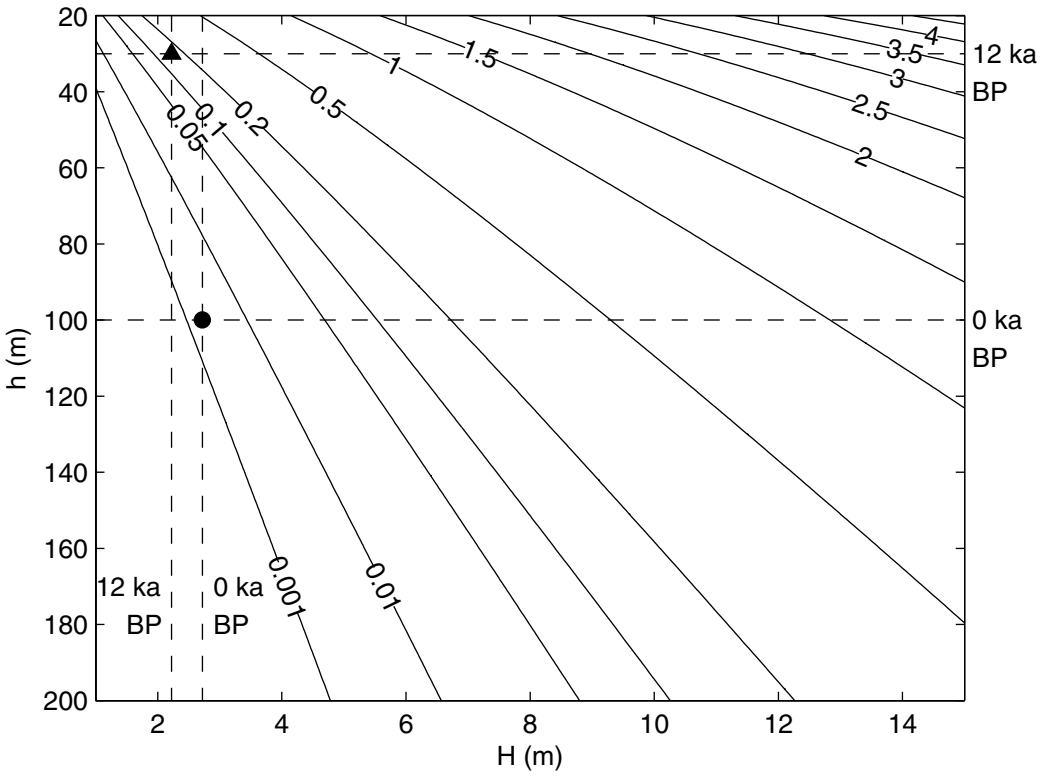
20
40
60
80
100
120
140
160
180
200
h (m)
2
4
6
8
10
12
14
H (m)
12 ka
BP
0 ka
BP
12 ka
BP
0 ka
BP
0.05
0.1
0.2
0.5
1
1.5
2
2.5
3
3.5
4
0.001
0.01

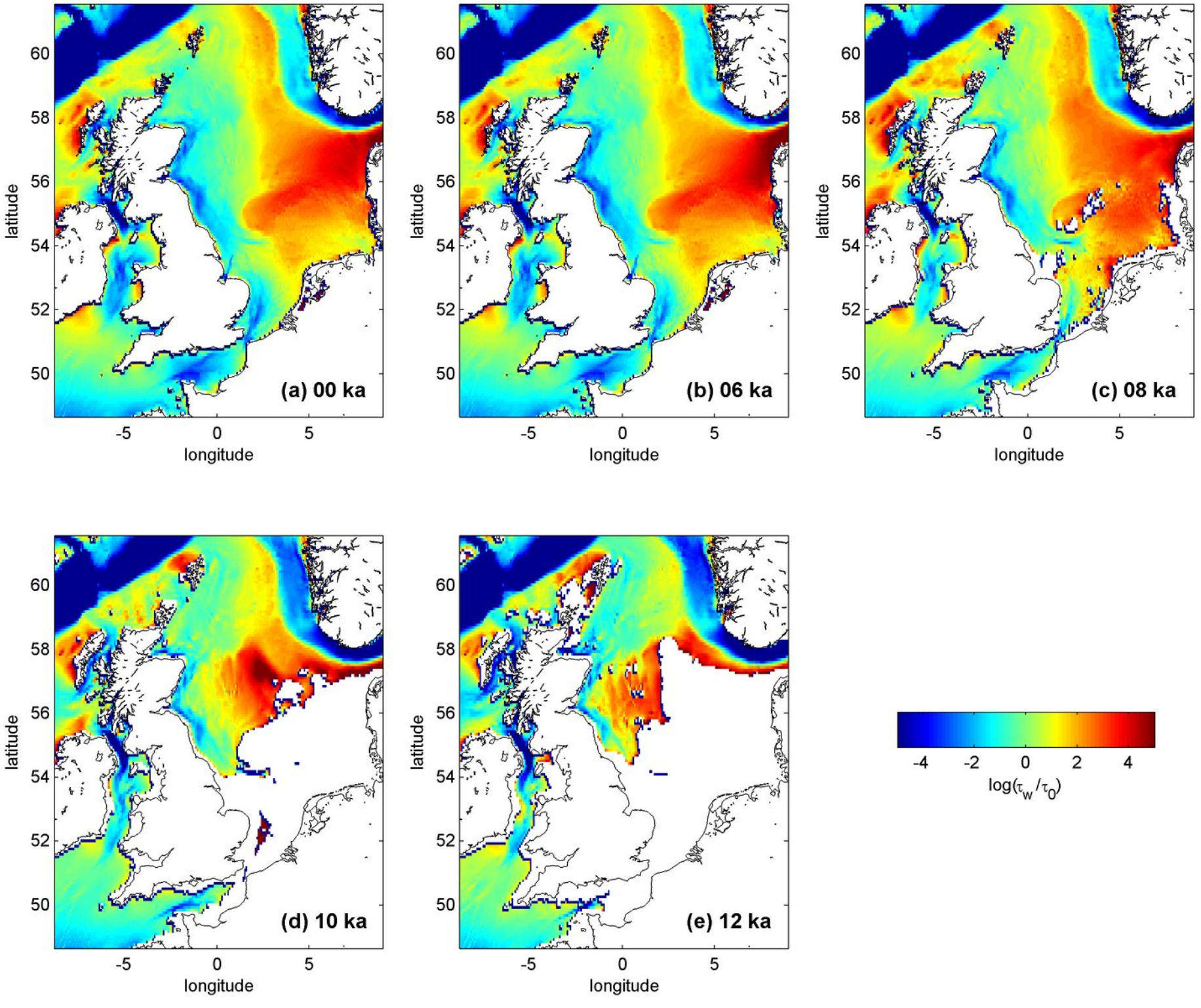
(a) 00 ka
(b) 06 ka
(c) 08 ka
(d) 10 ka
(e) 12 ka
latitude
longitude
60
58
56
54
52
50
-5
0
5
-4
-2
0
2
4
log(τw / τ0)

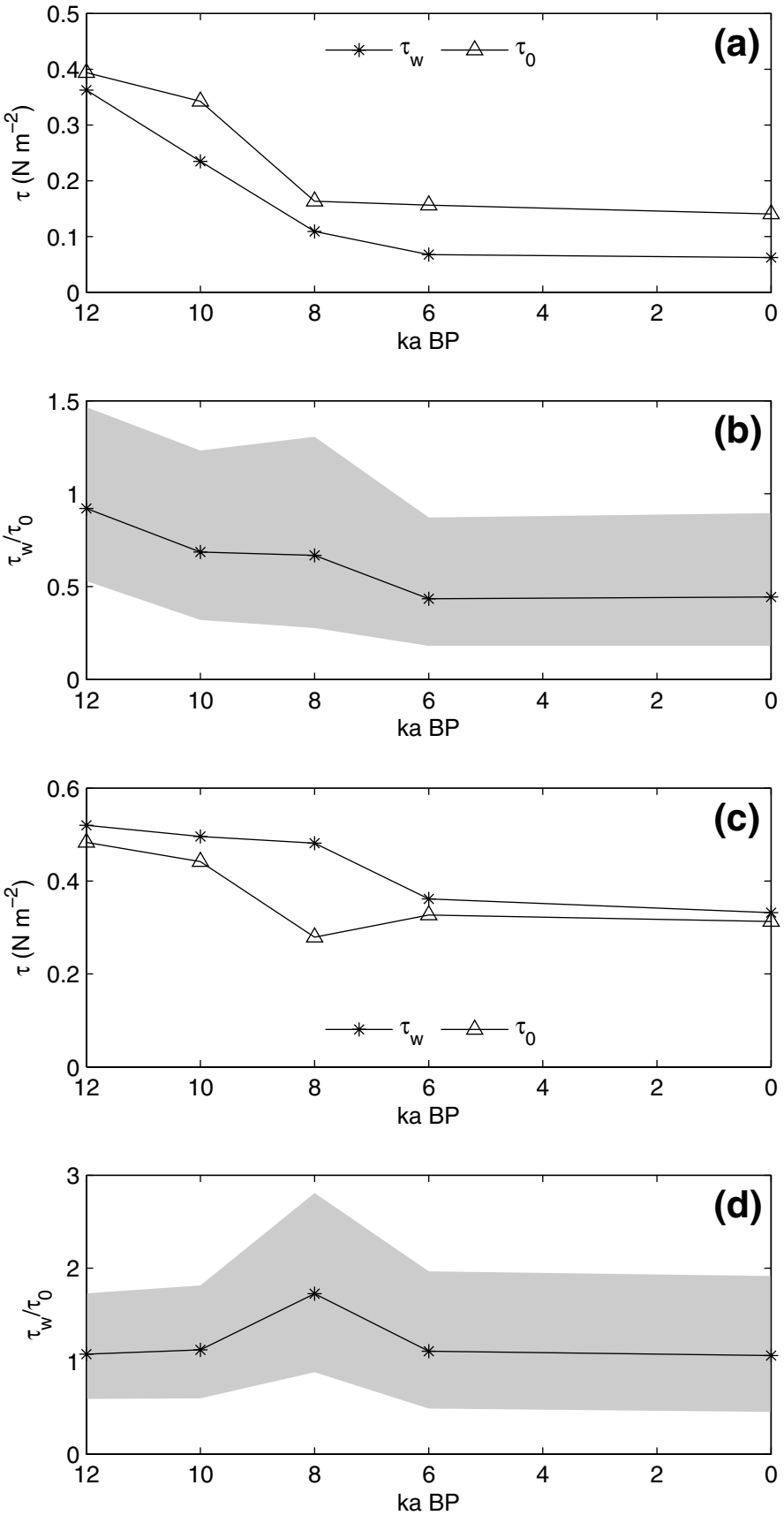
(a)
τw
τ0
τ (N m−2)
0.5
0.4
0.3
0.2
0.1
0
12
10
8
6
4
2
0
ka BP
(b)
τw/τ0
1.5
1
0.5
0
12
10
8
6
4
2
0
ka BP
(c)
τ (N m−2)
0.6
0.4
0.2
0
τw
τ0
12
10
8
6
4
2
0
ka BP
(d)
τw/τ0
3
2
1
0
12
10
8
6
4
2
0
ka BP